Indian Monsoonal Variations During the Past 80 Kyr Recorded in NGHP-02 Hole 19B, Western Bay of Bengal: Implications From Chemical and Mineral Properties

AGU100 ADVANCING EARTH AND SPACE SCIENCE

Geochemistry, Geophysics, Geosystems

RESEARCH ARTICLE
10.1029/2018GC007772

Key Points:
- The sedimentation rate was estimated for a sediment core from Hole 19B in the western Bay of Bengal, extending to approximately 80 kyr BP
- Indian monsoonal fluctuations on glacial-interglacial time scale implied from chemical and mineral properties
- Trace element ratios reflect changing in influences of the eastern and western branches of the Indian summer monsoon

Supporting Information:
- Supporting Information S1
- Data Set S1

Correspondence to:
Y. Ota,
ota@aori.u-tokyo.ac.jp

Citation:
Ota, Y., Kawahata, H., Kuroda, J., Yamaguchi, A., Suzuki, A., Araoka, D., et al. (2019). Indian monsoonal variations during the past 80 kyr recorded in NGHP-02 Hole 19B, western bay of Bengal: Implications from chemical and mineral properties. *Geochemistry, Geophysics, Geosystems*, *20*, 148–165. https://doi.org/10.1029/2018GC007772

Received 10 AUG 2018
Accepted 6 NOV 2018
Accepted article online 8 NOV 2018
Published online 6 JAN 2019

Indian Monsoonal Variations During the Past 80 Kyr Recorded in NGHP-02 Hole 19B, Western Bay of Bengal: Implications From Chemical and Mineral Properties

Yuki Ota[1,2,3,4], Hodaka Kawahata[1,2,3], Junichiro Kuroda[1,4], Asuka Yamaguchi[1,2], Atsushi Suzuki[3], Daisuke Araoka[3], Ayako Abe-Ouchi[1], Yasuhiro Yamada[5], Akira Ijiri[5], Toshiya Kanamatsu[5], Masataka Kinoshita[5], Kyaw Thu Moe[5], Weiren Lin[5], Saneatsu Saito[5], Yoshinori Sanada[5], Yohei Hamada[5], Yasuyuki Nakamura[5], Yuichi Shinmoto[5], Hung Yu Wu[5], Naokazu Ahagon[5], Kan Aoike[5], Koichi Iijima[5], Hideaki Machiyama[5], Maria Luisa Tejada[5], Keita Umetsu[5], Yoichi Usui[5], Yuzuru Yamamoto[5], Shuro Yoshikawa[5], Francisco Jimenez-Espejo[5], Satoru Haraguchi[5], Nobuharu Komai[5], Hisami Suga[5], Natsue Abe[5], Lallan Gupta[5], Takehiro Hirose[5], Yuka Masaki[5], Shun Nomura[5], Takamitsu Sugihara[5], Wataru Tanikawa[5], Yusuke Kubo[5], Lena Maeda[5], and Sean Toczko[5]

[1]Atmosphere and Ocean Research Institute, The University of Tokyo, Kashiwa, Japan, [2]Department of Earth and Planetary Science, The University of Tokyo, Tokyo, Japan, [3]Geological Survey of Japan, National Institute of Advanced Industrial Science and Technology (AIST), Tsukuba, Japan, [4]Department of Biogeochemistry, Japan Agency for Marine-Earth Science and Technology (JAMSTEC), Yokosuka, Japan, [5]NGHP-02 scientist team, Japan Agency for Marine-Earth Science Technology, Yokosuka, Japan

Abstract Detailed reconstruction of Indian summer monsoons is necessary to better understand the late Quaternary climate history of the Bay of Bengal and Indian peninsula. We established a chronostratigraphy for a sediment core from Hole 19B in the western Bay of Bengal, extending to approximately 80 kyr BP and examined major and trace element compositions and clay mineral components of the sediments. Higher $\delta^{18}O$ values, lower TiO_2 contents, and weaker weathering in the sediment source area during marine isotope stages (MIS) 2 and 4 compared to MIS 1, 3, and 5 are explained by increased Indian summer monsoonal precipitation and river discharge around the western Bay of Bengal. Clay mineral and chemical components indicate a felsic sediment source, suggesting the Precambrian gneissic complex of the eastern Indian peninsula as the dominant sediment source at this site since 80 kyr. Trace element ratios (Cr/Th, Th/Sc, Th/Co, La/Cr, and Eu/Eu*) indicate increased sediment contributions from mafic rocks during MIS 2 and 4. We interpret these results as reflecting the changing influences of the eastern and western branches of the Indian summer monsoon and a greater decrease in rainfall in the eastern and northeastern parts of the Indian peninsula than in the western part during MIS 2 and 4.

1. Introduction

The Indian monsoon is an important component of the Earth's climate system and affects more than 15% of the world's population. The development and sustenance of the agro-based economy on the Indian peninsula relies largely on rainfall from the Indian summer monsoon (Gadgil et al., 2005). The Indian monsoon has been predicted to change under global warming (Goswami et al., 2006; Malik et al., 2012). However, it is uncertain how changes to the Indian monsoon will affect regional precipitation, which exhibits complex patterns (Guhathakurta & Rajeevan, 2008). In this work, we aimed to reconstruct past regional precipitation patterns induced by Indian summer monsoonal variations, which will contribute to a better understanding of the climate system in this region.

The relationships between sediment transport and monsoons have been topics of intensive research (Krishnaswami & Tripathy, 2012; Saito et al., 2017; Singh et al., 2005; Tada et al., 2016). Major rivers draining the Himalaya and the Indian peninsula deliver approximately 1,350 Mt of sediment per year to the world's largest submarine fan in the Bay of Bengal, amounting to ~8% of the total riverine sediment supply to the world's oceans (Milliman, 2001; Milliman & Syvitski, 1992). In the Bay of Bengal, the Indian monsoon induces large seasonal variations in precipitation and runoff and seasonal reversals of the wind direction (Webster, 1987). More than 90% of the annual sediment load in rivers entering the Bay of Bengal results from rainfall

10.1029/2018GC007772

during the summer monsoon (Chakrapani & Subramanian, 1990a; Hart, 1999; Ota et al., 2017; Prasanna Kumar et al., 2007; Singh et al., 2007). Marine sediment records collected on scientific cruises (e.g., Tada & Murray, 2016) have revealed that the Indian monsoon has varied appreciably on glacial–interglacial and millennial time scales (Kathayat et al., 2016; Rashid et al., 2007; Tiwari et al., 2005). Studies of the sediment flux and chemical and isotopic characteristics of Bay of Bengal sediments have demonstrated that their origins in Himalayan river basins are largely regulated by climatic variations (Clift, 2017; Joussain et al., 2016; Kolla & Biscaye, 1973; Rao & Nath, 1988; Stoll et al., 2007). Moreover, climate change investigations have indicated that sediment supply to the Bay of Bengal and erosion and weathering patterns in Himalayan river basins are influenced by oscillations of the Indian summer monsoon and glacier cover in the higher Himalaya (Colin et al., 1999, 2006; Rahaman & Varis, 2009; Sinha et al., 2007; Tripathy et al., 2011).

The mineralogical and geochemical contributions of Indian peninsular rivers to Bay of Bengal sediments have recently received special attention (e.g., Bejugam & Nayak, 2016; Li, Liu, Feng, et al., 2017; Li, Liu, Shi, et al., 2017; Mazumdar et al., 2015; Phillips, Johnson, Giosan, & Rose, 2014; Phillips, Johnson, Underwood, et al., 2014). However, the erosion and weathering patterns in these river basins and their spatial and temporal variations on glacial–interglacial and millennial time scales remain poorly documented. In this study, we traced the origins of sediments at a core site in the western Bay of Bengal using variations in clay mineral content and major and trace element compositions to reconstruct the erosion and weathering histories of the source river basins. We apply our results to assess the role of climatic changes in regulating sediment transport in Indian peninsular river basins.

2. Geologic and Oceanographic Settings

2.1. Bay of Bengal

The Bay of Bengal contains the largest submarine fan in the world, extending ~3,000 km from north to south, ~1,400 km from east to west, and covering an area of ~3×10^6 km^2 (Curray et al., 2003). The bay has a maximum water depth of ~5,000 m (Curray et al., 2003) and is bordered by the Indian peninsula to the west, Bangladesh and the Himalaya to the north, and the Andaman Sea and Southeast Asia to the east (Figure 1). The Ganges-Brahmaputra river system discharges a high sediment load into the northern Bay of Bengal (~1×10^9 t/year) (Curray et al., 2003) and to the west, sediments are fed to the bay by several rivers, including the Mahanadi (~60×10^6 t/year), Godavari (~160×10^6 t/year), and Krishna rivers (~16×10^6 t/year; Ahmad et al., 2009; Tripathy et al., 2011). Peak precipitation during the Indian summer monsoon enhances these river discharges and increases sediment transport and physical and chemical weathering in these river catchments (e.g., Chakrapani & Subramanian, 1990a, 1990b; Hart, 1999; Ota et al., 2017; Prasanna Kumar et al., 2007; Singh et al., 2007). Once in the bay, riverine sediments are transported by surface and intermediate currents that flow counterclockwise in the northern Bay of Bengal during the winter, when winds are northeasterly, and clockwise during the summer, when winds are southwesterly (Figure 1; Chauhan & Vogelsang, 2006).

2.2. Climate and River Systems of the Indian Peninsula

The Indian peninsula comprises tropical to subtropical climate zones exhibiting strong seasonality dominated by tropical monsoon systems; climatic conditions are warm and humid during the summer and cold and dry during the winter. The Indian summer monsoon is divided into the Arabian Sea and Bay of Bengal branches. The Arabian Sea branch flows northward along the western margin of the Indian peninsula, delivering rain to coastal areas (Figure 1). The Bay of Bengal branch flows northward from the Bay of Bengal, delivering rain to the eastern and northeastern Indian peninsula (Figure 1). The central Indian peninsula does not receive much rain from the summer monsoon.

The Krishna-Godavari (K-G) basin, encompassing 28,000 km^2 on land and 145,000 km^2 offshore (Bastia, 2007; Rao, 2001), receives freshwater and sediments from the Krishna and Godavari rivers. The sediment load of these rivers is dominantly smectite (montmorillonite) with minor feldspar, quartz, kaolinite, and illite (Bejugam & Nayak, 2016; Rao, 1991; Subramanian, 1980). The Krishna River extends ~1,435 km from its origin in the Western Ghats at 1,337-m elevation and drains an area of 258,948 km^2 between 13°10′–19°22′N and 73°17′–81°9′E (Central Water Commission (CWC) and National Remote Sensing Centre (NRSC), 2014a). The major tributaries of the Krishna River are the Bhima and Tungabhadra Rivers, and the Ghataprabha and Malaprabha Rivers are minor tributaries. Bedrock in the Krishna catchment is 80% late Archean to early

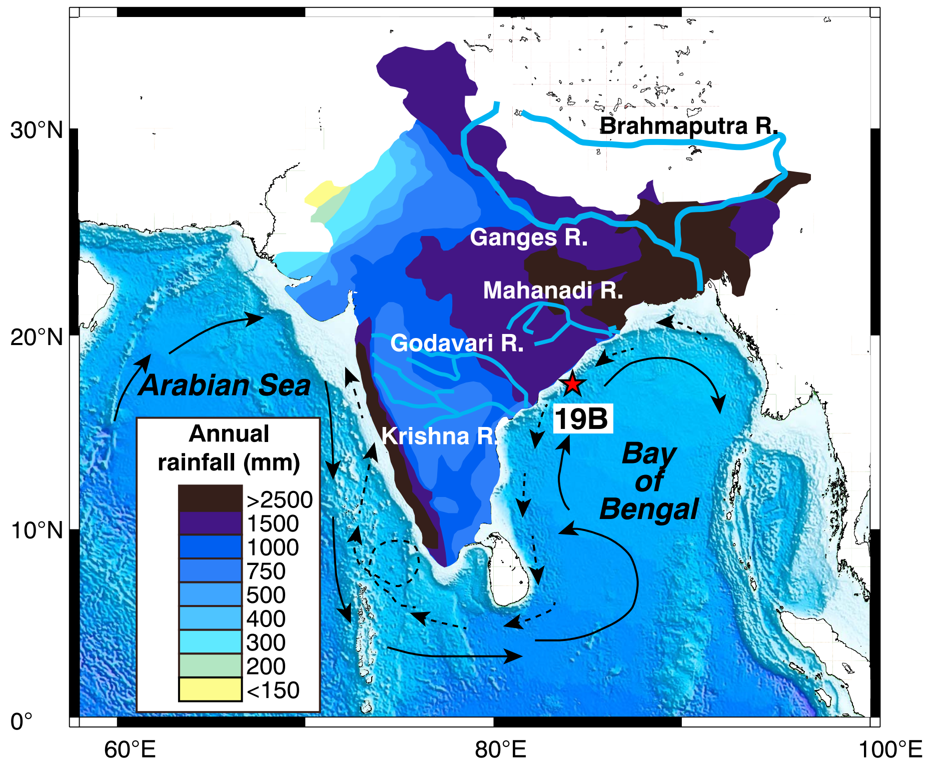

Figure 1. Location map showing Hole 19B in the western Bay of Bengal (red star) and mean annual precipitation across the Indian peninsula (simplified from Takahashi et al., 2008). Solid and dashed arrows represent the general summer and winter currents, respectively (Schott & McCreary, 2001).

Proterozoic gneissic rocks of the Eastern Ghats (granite, tonalite-trondjhemite-granodiorite, charnockite, and khondalite) and 20% Deccan basalts and younger Tertiary sediments (Ramesh et al., 1989). Average annual rainfall in the catchment is 859 mm, and the mean temperature is 26.7 °C (CWC and NRSC, 2014a). About 90% of the annual rainfall occurs during the summer monsoon.

The Godavari River extends ~995 km from its origin in the Western Ghats at 1,067-m elevation and drains an area of 302,065 km^2 between 16°19′–22°24′N and 73°24′–83°4′E (CWC and NRSC, 2014b). The Godavari River receives waters from the Darna, Pravara, and Manjra rivers on its right bank and from the Kadwa, Purna, Kaddam, Pranhita, Indravati, and Sabari rivers on its left bank (CWC and NRSC, 2014b). Rocks in its catchment include Deccan basalts (48%), the Precambrian gneissic complex (PGC, 39%), Proterozoic–Mesozoic sedimentary rocks of Gondwana affinity (11%), and recent alluvial cover (2%; Biksham & Subramanian, 1988; Meert et al., 2010). Average annual rainfall in the Godavari River catchment is 1,096 mm, of which about 90% occurs during the summer monsoon (CWC and NRSC, 2014b). Mean maximum and minimum temperatures are 33.0 and 20.8 °C, respectively. The mean annual temperature is 26.9 °C, though the western catchment is typically cooler than the eastern catchment (CWC and NRSC, 2014b).

The Mahanadi basin, fed by the Mahanadi River, covers ~260,000 km^2 and reaches water depths exceeding 3,000 m (Mazumdar et al., 2015). The Mahanadi River delivers ~66 km^3/year of freshwater (Tripathy et al., 2011) and sediment, including more illite and less smectite than sediments of the Krishna-Godavari river system plus minor chlorite, kaolinite, and gibbsite (Bejugam & Nayak, 2016; Mazumdar et al., 2015; Rao, 1991; Subramanian, 1980). Of its annual sediment discharge, 90% occurs during the Indian summer monsoon (Chakrapani & Subramanian, 1990b). The Mahanadi River extends ~850 km from its origin at 442-m elevation and drains an area of 142,000 km^2 between 19°20′−23°35′N and 80°30′−86°50′E (Jain et al., 2007). Important tributaries of the Mahanadi River are the Sheonath, Jonk, Hasdeo, Mand, Ib, Tel, and Ong Rivers. Rocks in its catchment include the PGC (56%), sedimentary rocks (limestone, shale, and sandstone, 39%), and recent alluvium and littoral deposits (5%) (Chakrapani & Subramanian, 1990a; Meert et al., 2010). Average annual

10.1029/2018GC007772

Table 1
Results of Radiocarbon Dating of Mixed Planktic Foraminifera in Sediment From Hole 19B

Core section	Depth in core (cm)	^{14}C age (year BP, 1σ)	δ^{13}C (‰VPDB)	Calibrated age (cal. year BP, 2σ)	Median age (cal. year BP)
1H-3	400.3	10,940 ± 30	1.74	12,380−12,614	12,516
1H-4	501.0	13,810 ± 40	2.90	15,957−16,287	16,133
1H-4	541.0	17,970 ± 40	2.48	20,999−21,435	21,222
1H-5	581.0	19,010 ± 45	1.61	22,355−22,600	22,466
1H-5	601.0	19,960 ± 60	1.94	23,311−23,804	23,560
1H-5	681.0	21,980 ± 60	3.50	25,726−26,007	25,866
1H-6	721.0	24,730 ± 70	3.87	28,123−28,773	28,383
1H-6	741.0	25,500 ± 80	2.25	28,863−29,433	29,133
1H-6	781.0	26,960 ± 80	4.17	30,642−31,013	30,829
1H-6	801.0	27,820 ± 90	3.55	31,080−31,435	31,259
1H-7	841.0	29,200 ± 90	0.58	32,591−33,361	32,970
1H-7	921.0	30,890 ± 100	1.46	34,169−34,727	34,458
1H-7	961.0	33,180 ± 120	1.55	36,289−37,238	36,671

rainfall is 1,110 mm and the mean maximum, minimum, and average temperatures are 32.3, 20.4, and 26.3 °C, respectively (CWC and NRSC, 2014c).

3. Materials and Methods

Samples analyzed in this study were obtained from the uppermost 18.12 m of the core recovered from Hole 19B (17°29′50.69″N, 84°13′42.75″E; ~80 km offshore) at a water depth of 2,520 m by D/V *Chikyu* during the Indian National Gas Hydrate Program Expedition 2 in 2015 (Figure 1). The lithology of the core is characterized by silty clay sediment, as explained in detail by Yamamoto et al. (2018). The core was split longitudinally into working and archive halves.

For age-dating purposes, we collected thirteen 2-cm-thick samples for microfossil and carbon isotopic (δ^{13}C) analyses by ^{14}C accelerator mass spectrometry at Paleo-Labo, Co., Ltd; sampling depths in the Hole 19B core are reported in Table 1. We also collected four 2-cm-thick sediment samples for total organic carbon (TOC) and δ^{13}C analyses by ^{14}C accelerator mass spectrometry at BetaAnalytic Co., Ltd; sampling depths for these samples are reported in Table 2. We report carbon isotopic compositions relative to Vienna Peedee Belemnite (VPDB) as $\delta^{13}C\ [‰] = [(^{13}C/^{12}C)_{sample}/(^{13}C/^{12}C)_{VPDB} - 1] \times 1,000$. In the Bay of Bengal, the large influx of fresh water results in steep gradients of the isopycnal surface within the top 200 m, preventing vertical mixing and advection of deeper ^{14}C-depleted water. Because the values of marine reservoir corrections in the Bay of Bengal are close to 400 years (Dutta et al., 2001; Southon et al., 2002), previous studies applied 400 years of marine reservoir age to radiocarbon ages of planktic foraminifera (e.g., Govil & Naidu, 2011; Joussain et al., 2016; Phillips, Johnson, Giosan, & Rose, 2014; Ponton et al., 2012). Therefore, we adopted 400 years as the marine reservoir age for this core. Radiocarbon ages were converted to calendar ages (expressed in cal. yr BP) using the Marine13 database (Reimer et al., 2013) and Calib v. 7.1 program (Stuiver et al., 2017).

To isolate foraminifera from the coarse fraction of the sediments, we collected seventy 2-cm-thick samples (sampling depths in the core are reported in Table S1 in the supporting information) and wet sieved them using a 63-μm mesh. Then, tests of the foraminifer *Globigerinoides ruber* sensu stricto (*G. ruber* s. s.) measuring 250–350 μm and weighing 70–100 μg were obtained from the >63-μm size fraction; this size range was used to minimize ontogenetic and growth rate effects on shell geochemistry (Lea et al., 2000; Spero et al., 2003). The sampled depth in core from Hole 19B was represented in the supporting information (Table S1). The foraminifera were sonicated in methanol for ~30 s to remove foreign material from their interiors. Foraminifer samples were reacted with 100% H_3PO_4 at 25 °C in a custom-made carbonate preparation device (Ishimura et al., 2004), and their oxygen isotopic ratios were measured with an Isoprime Micromass stable isotope ratio mass spectrometer at the National Institute of Advanced Industrial Science and Technology. Measurements were calibrated using international reference standard NBS 19. We report oxygen isotopic compositions relative to VPDB as $\delta^{18}O\ [‰] = [(^{18}O/^{16}O)_{sample}/(^{18}O/^{16}O)_{VPDB} - 1] \times 1,000$, adopting the consensus value of −2.20‰ for NBS 19 relative to VPDB. The δ^{18}O precision was better than 0.1‰ (1σ).

 10.1029/2018GC007772

Table 2
Results of Radiocarbon Dating of Sediment TOC Samples From Hole 19B

Core section	Depth in core (cm)	^{14}C age (year BP, 1σ)	δ^{13}C (‰VPDB)	Calibrated age (cal. year BP, 2σ)	Median age (cal. year BP)
1H-1	76.5	3,070 ± 30	−20.2	2,751−2,926	2,832
1H-3	370.3	12,620 ± 40	−18.3	13,960−14,250	14,106
1H-7	841.0	27,480 ± 90	−16.2	30,909−31,260	31,090
1H-7	961.0	29,730 ± 110	−16.6	33,277−33,850	33,581

Fifty-nine 2-cm-thick samples were collected, freeze-dried, and then ground and homogenized with an agate mortar for organic matter and mineral content analyses. The sampling depths of these samples are reported in Table S2. We measured total carbon (TC), TOC, and total nitrogen (TN) contents (wt.%) using a Flash 2000 CHNS elemental analyzer at the Geological Survey of Japan (GSJ) following analytical methods similar to those of Ota et al. (2017). We weighed powdered samples (~30 mg) in a Sn sample boat for TC and TN measurements. For TOC determination, a ~30-mg portion of the dried sample was decalcified in a Ag sample boat with a few drops of 1 N HCl and dried for at least 2 hr at 80 °C to remove unreacted HCl and water. The dried and decalcified samples were then wrapped in a Sn sample boat for combustion. In sediments of the western Bay of Bengal, carbonate is considered to be solely foraminiferal calcium carbonate (e.g., Phillips, Johnson, Giosan, & Rose, 2014; Tripathy et al., 2014). Therefore, the carbonate content was calculated as follows:

$$\text{carbonate } [\text{wt.}\%] = (100/12) \times (\text{TC} - \text{TOC}) \quad (1)$$

Based on five replicate analyses, analytical errors were within 1% for all analyses.

The mineral composition of the clay fraction (<2 μm) was determined by X-ray diffraction in nineteen 2-cm-thick samples; sampling depths are reported in Table S3. Samples were treated with 10% H_2O_2 and 1 N HCl to remove organic matter and calcium carbonate, respectively, and then centrifuged at 1,000 revolutions per minute for 2.4 min, following the method of Phillips, Johnson, Underwood, et al. (2014). Clay minerals were analyzed at GSJ using a Rigaku Rint 2500 X-ray diffractometer with Cu Kα radiation. We saturated the oriented samples with ethylene glycol using a vapor chamber heated to 60 °C prior to X-ray diffraction analyses. Scans were performed at 40 kV and 100 mA with 2θ ranging from 3 to 35° at a rate of 1°/min and a step size of 0.01°. Clay minerals were identified based on the following peak areas: smectite (001) at ~5.3°2θ, illite (001) at ~8.93°2θ, and the composite [kaolinite (001) + chlorite (002)] at ~12.53°2θ. We followed the traditional approach of Biscaye (1965) for calculation of relative clay abundances based on peak area values and used factors of 1, 4, and 2 for smectite, illite, and [kaolinite (001) + chlorite (002)], respectively. Errors were estimated to be less than 10% of the relative abundance of each clay mineral.

Sixty 2-cm-thick sediment samples were collected and filtered to <63 μm for sediment provenance and weathering determinations; sampling depths are reported in Table S4. Carbonate and apatite, and organic matter were removed using 1 N HCl and 30% H_2O_2 for 24 hr, respectively, and further analytical methods were similar to those of He et al. (2015) and Suzuki et al. (2016). To desalinate the sample, the supernatant was removed, Milli-Q water was added, and the sample was centrifuged for 10 min at 2,500 revolutions per minute; this procedure was performed 3 times. After drying at 60 °C, the samples were ground to a fine powder in an agate mortar. About 0.5 g of the powdered samples were ignited and fused with approximately 5 g of lithium tetraborate to make glass beads for major and trace element analyses. Major elements were analyzed on a Rigaku ZSX-Primus II X-ray fluorescence spectrometer at the Atmosphere and Ocean Research Institute, The University of Tokyo, using a 50-kV excitation voltage and 50-mA current. Element contents were calculated as a percentage of the counts per second. Based on six replicate analyses, relative standard deviations of the measurements were 0.03% for SiO_2, 0.19% for TiO_2, 0.06% for Al_2O_3, 0.04% for Fe_2O_3, 4.81% for MnO, 0.40% for MgO, 0.19% for CaO, 0.85% for Na_2O, 0.04% for K_2O, and 6.17% for P_2O_5. Trace element contents were determined by laser ablation inductively coupled plasma mass spectrometry at GSJ, using a custom-built laser sampling system interfaced between a New Wave Research NWR213 laser ablation system and an Agilent 7700× quadrupole inductively coupled plasma mass spectrometry. The laser ablation system consists of a Nd:YAG laser that generates an output wavelength of 213 nm and a maximum pulse energy of >30 J/cm^2; detailed information about the instrument is given in Yamasaki and Yamashita

Table 3
Estimated Ages of Sediment Samples From Hole 19B Based on Marine Isotope Events in the $\delta^{18}O$ Record of Globigerinoides ruber s.s. Ages of the $\delta^{18}O$ Stacks Follow Lisiecki and Raymo (2005)

Core section	Depth in core (cm)	Age (kyr)
1H-4	511.0	18
2H-1	1,086.0	45
2H-3	1,366.0	52
2H-4	1,426.0	55
2H-4	1,526.0	64
2H-5	1,606.0	69

(2016). Laser ablation was performed using a 100-μm laser spot size, a repetition rate of 10 Hz, a laser energy of ~20 J/cm^2, a rastered area of 500 μm × 500 μm, and a raster speed of 20 μm/s. The accuracy and precision of laser ablation related specifically to the analytical protocols used for glass beads are described in detail in Yamasaki and Yamashita (2016).

4. Results

4.1. Dating and Sedimentation Rate

Thirteen calibrated radiocarbon ages of mixed planktic foraminifera from the Hole 19B sediment core were calculated (Table 1). We also determined four calibrated radiocarbon ages of sediment TOC samples (Table 2), three of which (at 370.3-, 841.0-, 961.0-cm depth) could be compared to foraminifer ages from the same core depth. The absolute differences (relative percent differences in parentheses) in calibrated radiocarbon ages of TOC from foraminifers in these three samples were −2,105 years (−13.1%), 1,299 years (5.7%), and 3,151 years (8.4%), respectively. Using this average difference, we adjusted the calibrated radiocarbon age at 76.5-cm depth to 40% higher than the sediment TOC age (2,832 cal. year BP) at the same depth, that is, to 3,944 cal. year BP. The $\delta^{18}O$ values from *G. ruber* s.s. ranged from −3.51 to −0.66‰ (average −1.55‰, n = 70, σ = 0.53‰; Table S1). We constructed an age model via manual graphical correlation of the $\delta^{18}O$ record from *G. ruber* s.s. to the LR04 global benthic $\delta^{18}O$ stack (Lisiecki & Raymo, 2005) using Match 2.3 (Lisiecki & Lisiecki, 2002). To match both records and estimate the sedimentation rate using Match 2.3, 13 planktic foraminifera and TOC-calibrated radiocarbon age points and six $\delta^{18}O$ stack age points (Table 3) were configured as age tie points and plotted in Figure 2b. A nondispersed prominent volcanic ash layer observed at 17.7–17.9-m depth was deposited approximately 74 kyr according to our age model, which agrees well with published estimates for the timing of the Toba volcanic eruption (73.88 ± 0.32 ka; Scudder et al., 2016; Storey et al., 2012). Our age model shows the chronostratigraphy for the ~80-kyr record of the sediment core. The established sedimentation rates between samples derived with this model range from 8 to 41 cm/kyr, averaging 30 cm/kyr (Figure 2b). We classified the core sediments into five units based on the ages of marine isotope stages (MIS) (Lisiecki & Raymo, 2005) in ascending order: MIS 1, 0–385.3 cm (0–12 cal. kyr BP); MIS 2, 385.3–731.0 cm (12–29 cal. kyr BP); MIS 3, 731.0–1,386.0 cm (29–56 cal. kyr BP); MIS 4, 1,386.0–1,696.0 cm (56–71 cal. kyr BP); MIS 5, 1,696.0–1,986.0 cm (before 71 cal. kyr BP).

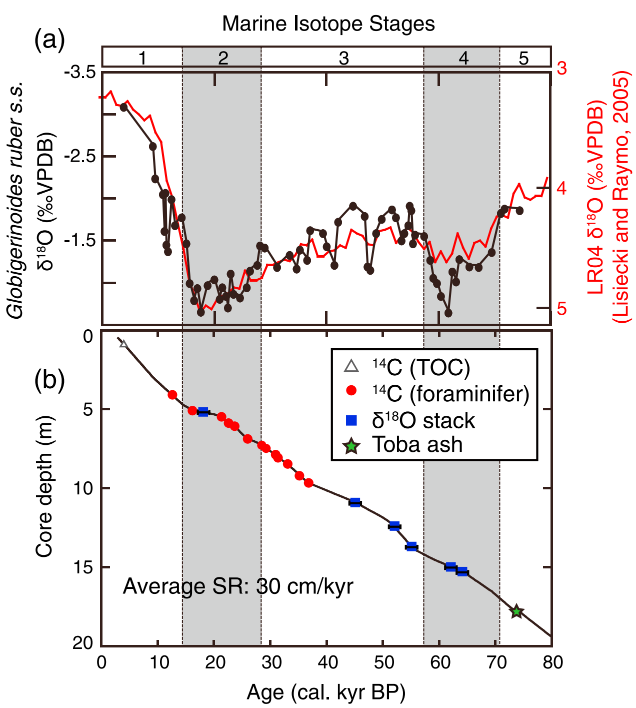

Figure 2. (a) Correlation of the $\delta^{18}O$ records of *Globigerinoides ruber* s.s. from Hole 19B (black symbols and line) and the LR04 global benthic $\delta^{18}O$ records (red line; Lisiecki & Raymo, 2005). (b) Age depth diagram of Hole 19B. The average sedimentation rate (SR) of the core is 30 cm/kyr. VPDB = Vienna Peedee Belemnite; TOC = total organic carbon.

4.2. TC, TOC, TN, C/N Ratio, and Carbonates

TC, TOC, TN, C/N ratios, and carbonate contents of the 59 samples analyzed are presented in Table S2. Carbonate contents in the Hole 19B sediments vary widely, ranging from 0.5 to 58.4 wt.% (average 15.7 wt.%, σ = 13.2 wt.%). Carbonate contents showed changes related to glacial-interglacial cyclicity, with higher values during MIS 2 and 4 than MIS 1, 3, and 5 (Figure 3e). TC contents ranged from 1.3 to 7.7 wt.% (average 3.2 wt.%, σ = 1.5 wt.%), TOC contents from 0.7 to 2.8 wt.% (average 1.4 wt.%, σ = 0.4 wt.%), TN contents from 0.11 to 0.20 wt.% (average 0.15 wt.%, σ = 0.02 wt.%), and the molar ratio of TOC/TN (C/N) ranged from 3.9 to 21.5 (average 8.2, σ = 2.5).

4.3. Clay Mineral Compositions

Relative clay mineral abundances in the 19 samples analyzed are presented in Table S3. Illite was the dominant clay mineral, accounting for 33–64% (average 48%, σ = 6%). The relative smectite abundances were 5–26% (average 18%, σ = 6%), and chlorite and kaolinite accounted for 22–46% of the clays (average 35%, σ = 7%).

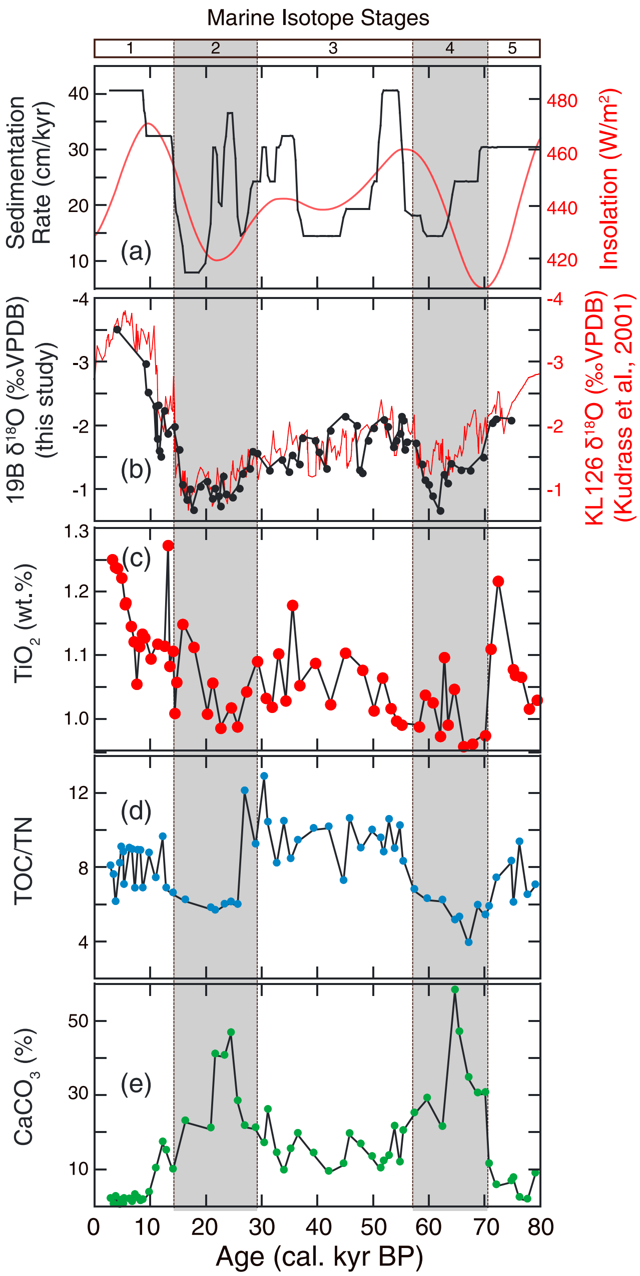

Figure 3. Time series profiles of Hole 19B: (a) Sedimentation rate (black line) and 21 July insolation at 65°N (red line; Berger, 1978), (b) $\delta^{18}O$ records of *Globigerinoides ruber* s.s. from Hole 19B (black line) and KL126 (red line; Kudrass et al., 2001), (c) TiO_2 content, (d) TOC/TN ratios, and (e) $CaCO_3$ content. VPDB = Vienna Peedee Belemnite; TOC = total organic carbon; TN = total nitrogen.

4.4. Major and Trace Elements

The major element compositions of the 60 sediment samples analyzed are presented in Table S4. SiO_2 content varied from 61.51 to 76.33 wt.% (average 68.97 wt.%, σ = 3.11 wt.%), TiO_2 from 0.96 to 1.28 wt.% (average 1.08 wt.%, σ = 0.08 wt.%), Al_2O_3 from 16.77 to 22.21 wt.% (average 18.72 wt.%, σ = 1.29 wt.%), Fe_2O_3 from 2.42 to 8.59 wt.% (average 4.99 wt.%, σ = 2.07 wt.%), MnO from 0.01 to 0.07 wt.% (average 0.02 wt.%, σ = 0.02 wt.%), MgO from 0.86 to 2.44 wt.% (average 1.36 wt.%, σ = 0.46 wt.%), CaO from 0.24 to 0.77 wt.% (average 0.46 wt.%, σ = 0.14 wt.%), Na_2O from 0.27 to 0.75 wt.% (average 0.46 wt.%, σ = 0.16 wt.%), K_2O from 2.61 to 3.70 wt.% (average 3.11 wt.%, σ = 0.23 wt.%), and P_2O_5 from 0.02 to 0.14 wt.% (average 0.06 wt.%, σ = 0.03 wt.%). Ti content variations showed changes related to glacial-interglacial cyclicity, with higher Ti contents during MIS 1, 3, and 5 than during MIS 2 and 4 (Figure 3c).

The trace element concentrations of the 60 sediment samples are presented in Table S4 and chondrite-normalized rare earth element (REE) patterns are shown in Figure 6. Cr contents varied from 72.31 to 158.45 ppm (average 101.45 ppm, σ = 18.04 ppm), Co from 3.33 to 75.54 ppm (average 9.26 ppm, σ = 9.32 ppm), La from 26.17 to 47.69 ppm (average 33.03 ppm, σ = 5.62 ppm), and Th from 10.16 to 33.90 ppm (average 21.50 ppm, σ = 6.91 ppm). Cr/Th, Th/Sc, Th/Co, and La/Cr ratios were 3.2–10.7, 0.7–1.8, 0.4–6.7, and 0.2–0.4, respectively (Figures 5a–5d). Variations in the Th/Co, La/Cr, and Cr/Th ratios showed changes related to glacial-interglacial cyclicity, with Th/Co, Th/Sc, and La/Cr ratios being lower and Cr/Th being higher during glacial periods. The Eu anomaly was calculated using the formula of Seto and Akagi (2008):

$$Eu/Eu^{*} = Eu_N/(Sm \times Gd)_N^{\ 1/2} \tag{2}$$

where the subscript N indicates C1 chondrite-normalized values. In general, the chondrite-normalized REE patterns of the studied samples appear similar (Figure 6), characterized by high light REE/heavy REE (LREE/HREE) ratios, almost flat HREE patterns, and pronounced but variable Eu anomalies. The analyzed samples have Eu/Eu* values in the range of 0.52–0.72 and show glacial-interglacial cyclicity, with higher Eu/Eu* ratios during glacial periods (Figure 5d).

5. Discussion

5.1. Hydrological Conditions Influenced by the Indian Monsoon

Oceanic sediments dominated by clastic materials are generally characterized by high sedimentation rates and dilution of the biogenic components by the terrestrial influx (Einsele, 2000). The sedimentation rate at Hole 19B during the past 80 kyr ranged from 8 to 41 cm/kyr (Figure 3a), averaging 30 cm/kyr, which is higher than at other core sites in the Bay of Bengal (Sijinkumar, 2016). This higher sedimentation rate indicates a strong terrestrial influx at Hole 19B. Sea surface temperature (Figure 3a) or salinity variations seem to have affected the $\delta^{18}O$ values of seawater and calcite. In the Bay of Bengal, previous studies reported that the $\delta^{18}O$ values of *G. ruber* s.s. primarily reflect salinity variations, which are attributed to the freshwater influx from rivers and precipitation (e.g., Colin et al., 1999; Evans et al., 2015; Kudrass et al., 2001; Ponton et al., 2012; Sengupta et al., 2013; Stoll et al., 2007). The *G. ruber* s.s. $\delta^{18}O$ record at Hole 19B varied on glacial-interglacial time scales, with lower values during MIS 1, 3, and 5 (Figure 3b), indicating that the summer monsoon brought more precipitation to the western Bay of Bengal during those periods. The TiO_2 profile at Hole 19B also varied on glacial-interglacial time scales, with higher values during MIS 1, 3, and 5 (Figure 3c). Though sediment TiO_2 contents are complicatedly linked with provenance and size-sorting (i.e., the energy condition during transport; Schmitz, 1987; Wei et al., 2003; Yarincik et al., 2000), modern seafloor sediments in the western Bay of Bengal have higher TiO_2 contents near river mouths, where terrestrial input increases with stream energy (Bejugam & Nayak, 2016). Furthermore, C/N ratios show a trend similar to that of TiO_2 content and opposite that of biogenic carbonate content (Figures 3d and 3e). In general, the C/N ratio of marine phytoplankton is close to 6.7, whereas that of terrestrial vascular plants exceeds 12 (Lamb et al., 2006). Therefore, these results suggest a high detrital input into the western Bay of Bengal during MIS 1, 3, and 5, consistent with increased monsoonal precipitation during those periods.

At millennial to glacial-interglacial time scales, changes in the transport of lithogenic sediments can be caused by sea level variations and river flow fluctuations (e.g., Awasthi et al., 2014; Colin et al., 2006; Joussain et al., 2016). Precessional variance of the Northern Hemisphere summer insolation induced greater ice volumes and lower sea levels during MIS 2 and 4 (Berger, 1978). During low stands, rivers in the lower reaches of the drainage system are constricted to their main channels and transfer sediment to the open ocean more efficiently (e.g., Awasthi et al., 2014; Colin et al., 2006). However, our results imply that the influx of detrital material was greater in MIS 1, 3, and 5, when sea level was relatively high. This finding suggests that sediment transport to our core site was little influenced by sea level and was primarily controlled by river discharge, which was driven in turn by summer monsoonal precipitation (Chakrapani & Subramanian, 1990b; Prasanna Kumar et al., 2007; Subramanian, 1993). Among these interglacial stages, the $\delta^{18}O$ values of *G. ruber* s.s. and $CaCO_3$ contents were lowest and the TiO_2 content of sediments were highest during MIS 1. *Globigerinoides ruber* s.s. $\delta^{18}O$ records in core KL126 also showed their lowest values of the last 80 kyr during MIS 1 (Kudrass et al., 2001; Figure 3b). Therefore, we infer that during the last 80 kyr, Indian summer monsoonal precipitation in the western Bay of Bengal was the most extreme during MIS 1. Previous studies have also connected enhanced monsoonal precipitation and increased Northern Hemisphere summer insolation during MIS 1, 3, and 5 (Kathayat et al., 2016; Phillips, Johnson, Giosan, & Rose, 2014; Rashid et al., 2011; Figure 3a). Indeed, the modeling study of Broccoli et al. (2006) has proposed that increased summer insolation in the Northern Hemisphere results in the northward displacement of the intertropical convergence zone (ITCZ) and strengthens summer monsoons.

5.2. Weathering and Sediment Maturity

Sediment geochemical compositions are widely used to infer weathering conditions in the source area, and sorting and maturity during transport (Armstrong-Altrin & Machain-Castillo, 2016; Fedo et al., 1995). We evaluated weathering intensity from the molar compositions of the sediments (60 samples) using the Chemical Index of Alteration (CIA = $100 \times [Al_2O_3/(Al_2O_3 + CaO + Na_2O + K_2O)]$; Nesbitt & Young, 1982), the Chemical Index of Weathering (CIW = $100 \times [Al_2O_3/(Al_2O_3 + CaO + Na_2O)]$; Harnois, 1988), and the Plagioclase Index of Alteration (PIA = $100 \times [(Al_2O_3 - K_2O)/(Al_2O_3 + CaO + Na_2O)]$; Fedo et al., 1995), where CaO values signify the CaO content of silicate minerals alone. As our samples were treated with 1 N HCl to remove carbonate and apatite, our reported CaO contents can be used to calculate these weathering indices.

Unweathered igneous rocks have CIA and CIW values below 50%, Phanerozoic shales have values from 70% to 75%, and residual clays (kaolinite, chlorite, and gibbsite) have values near 100% (Nesbitt & Young, 1984). Deccan basalts and their weathering products have CIA values of ~35% and ~100%, respectively (Babechuk et al., 2014). Gneissic complex rocks and their weathering products have CIA values of ~46% and ~88–96%, respectively (Tripathi & Rajamani, 2007). Core sediments from Hole 19B have CIA values between 75% and 82% (average 79%, $\sigma = 2$) and CIW values between 88% and 95% (average 92%, $\sigma = 2$) (Figures 4a and 4b). The average CIA values during MIS 1–5 were 81%, 78%, 79%, 76%, and 80%, respectively, and the average CIW values were 94%, 91%, 92%, 89%, and 93%, respectively. Sediments deposited during MIS 2 and 4 have comparatively low CIA and CIW values, indicating a lower intensity of weathering in the source area than during MIS 1, 3 and 5.

Fresh plagioclase has PIA values below 50%, and the PIA value increases with increased weathering intensity (Fedo et al., 1995). Weathered and parent gneissic complex rocks have PIA values of ~87–96% and ~40%, respectively, and weathered and parent Deccan basalts have PIA values of ~100% and ~33%, respectively

10.1029/2018GC007772

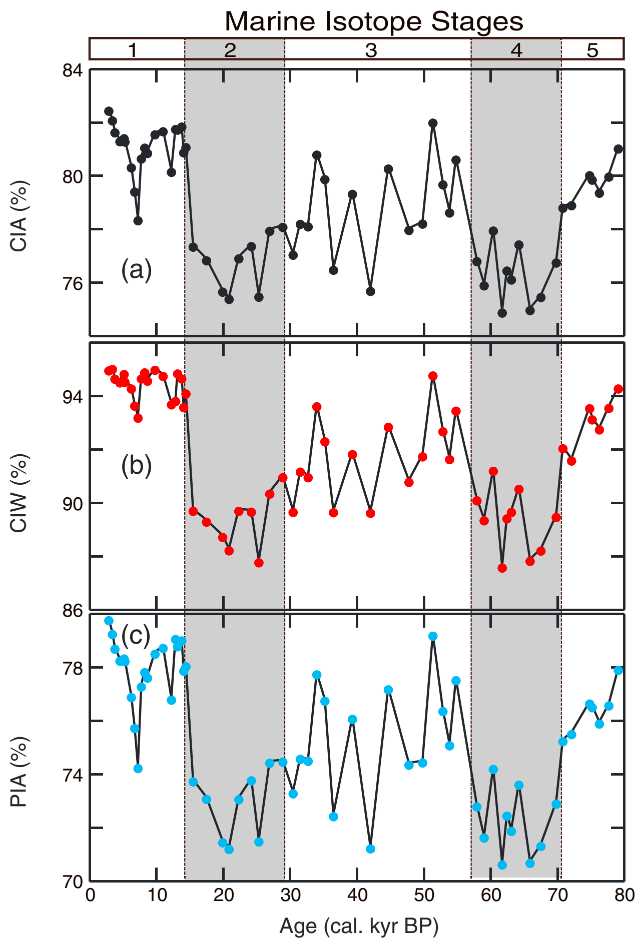

Figure 4. Time series profiles of sedimentary weathering indices from Hole 19B: (a) Chemical Index of Alteration (CIA), (b) Chemical Index of Weathering (CIW), and (c) Plagioclase Index of Alteration (PIA).

(Tripathi & Rajamani, 2007). The PIA values of Hole 19B sediments ranged from 71% to 80% (average 75%, $\sigma = 2$). The average PIA values during MIS 1–5 were 78%, 74%, 75%, 72%, and 76%, respectively. The PIA values were lower during MIS 2 and 4 than during MIS 1, 3, and 5 (Figure 4c). Therefore, all three weathering indices indicate very intense weathering in the source area during MIS 1, 3, and 5 and less intense weathering during MIS 2 and 4. Our TiO_2 content profile indicates that the summer monsoon brought more precipitation to the areas surrounding the western Bay of Bengal during MIS 1, 3, and 5 than during MIS 2 and 4. These results are in agreement with the indications of strong weathering in the source area during these periods because chemical weathering is enhanced by increased monsoonal precipitation (Colin et al., 1999, 2006; Hecht & Oguchi, 2017; Limmer et al., 2012; Miriyala et al., 2017). However, Blöthe and Korup (2013) estimated the lag times between erosion of Himalayan and Tibetan sources and marine deposition to be 10–100 kyr. If such lag times are applicable to the Hole 19B sediments, then the chemical and mineral compositional variations of sediments in the Bay of Bengal cannot be attributed to varying intensities of physical and chemical weathering of their source rocks. Future work on geochemical weathering should provide more direct indicators of chemical and physical weathering.

5.3. Probable Sediment Sources

In the Bay of Bengal, smectite-rich sediments are thought to originate dominantly from mafic igneous rocks such as the Deccan basalts via the Krishna and Godavari rivers, whereas illite-rich sediments are thought to originate from felsic rocks such as the PGC of the eastern Indian peninsula and Himalayan rocks (e.g., Alagarsamy, 2009; Bejugam & Nayak, 2016; Mazumdar et al., 2015; Rahman & Suzuki, 2007).

The composition of clastic sediments is controlled primarily by the original composition of the source rocks; therefore, major and trace element geochemistry provides information about the origin of sediments and weathering conditions in their source area (Armstrong-Altrin & Machain-Castillo, 2016; Fedo et al., 1995). Sediment trace element contents have been widely used to investigate sediment provenance (Ali et al., 2014; Cullers, 2002), and several trace elements, such as REEs, Th, Cr, and Co, are most suited to this purpose because of their relatively low mobility during weathering and other sedimentary processes and their short residence times in seawater (Cullers et al., 1979). High field strength elements (La and Th) are primarily concentrated in felsic igneous rocks (Feng & Kerrich, 1990), whereas ferromagnesian transition elements (Sc, Cr, and Co) are concentrated in mafic igneous rocks (Armstrong-Altrin et al., 2015; Cullers, 2002). Accordingly, elemental ratios and diagrams based on these elements are useful in discriminating sediment provenance. Ratios of relatively immobile trace elements, such as Cr/Th, Th/Co, Th/Sc, and La/Cr, are considered to be useful proxies of source compositions (Ali et al., 2014; Cullers, 2002). In sediments derived from felsic and mafic rocks, Cr/Th ratios are generally 4–15 and 25–500, respectively, Th/Sc ratios are more and less than 1, respectively, and Th/Co ratios are 0.7–19.4 and 0.0–1.4, respectively (Ali et al., 2014). Felsic rocks have higher La/Cr ratios than mafic rocks (Ali et al., 2014). The Cr/Th, Th/Co, Th/Sc, and La/Cr ratios of Indian peninsula granite and gneiss are 0.8–9.1, 1.6–13.9, 0.9–6.2, and 0.1–1.1, respectively (Garzanti et al., 2010; Stummeyer et al., 2002); for Deccan basalts, those ratios are 5.1–167.6, 0.0–0.2, 0.0–0.2, and 0.0–0.1, respectively (Melluso et al., 2004; Shukla et al., 2001). Although Himalayan source rocks contain felsic and mafic rocks, Ganges-Brahmaputra sediments have ratios generally similar to those of felsic source sediments (Cr/Th = 0.8–9.1, Th/Co = 0.7–13.9, Th/Sc = 1.9–6.2, and La/Cr = 0.6–2.9, Garzanti et al., 2010). Hole 19B sediments have ratios consistently in or near the ranges of the PGC and Ganges-Brahmaputra sediments (Cr/Th = 3.2–10.7, Th/Sc = 0.7–1.8, Th/Co = 0.4–6.7, and La/Cr = 0.2–0.4; Figures 5a–5d). These results indicate the dominant transport of sediments from the PGC and Himalayan rocks to Hole 19B during the last 80 kyr, consistent with previous studies showing that

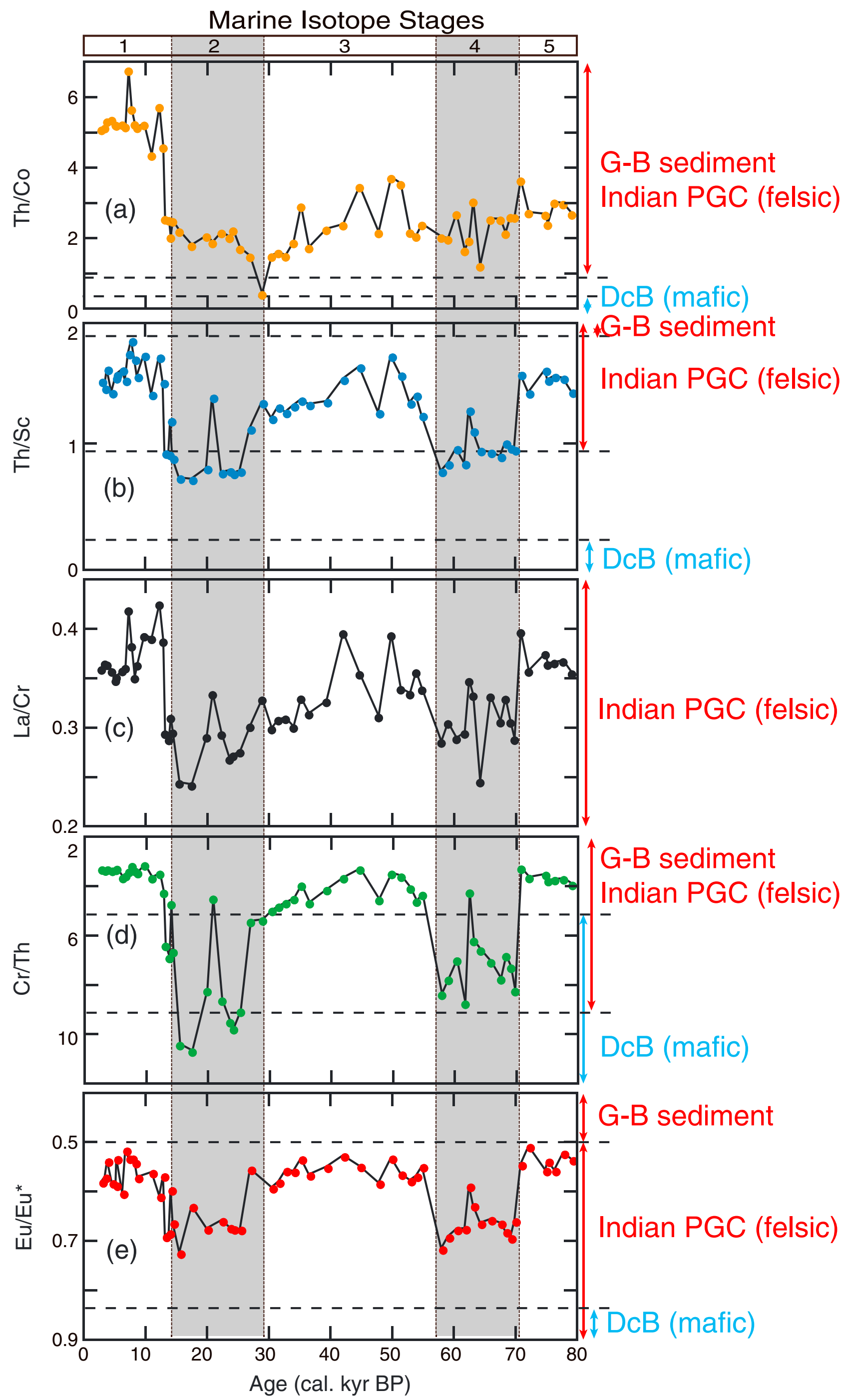

Figure 5. Time series trace element profiles of the Hole 19B core: (a) Th/Co, (b) Th/Sc, (c) La/Cr, (d) Cr/Th, and (e) Eu/Eu*. Boundary values between Ganges-Brahmaputra sediments (Garzanti et al., 2010), the Indian Precambrian Gneiss Complex (PGC; Moyen et al., 2003), and Deccan Basalts (DcB; Krishnamurthy et al., 2014; Melluso et al., 2004; Shukla et al., 2001) are shown by dashed lines in each panel, and the ranges are labeled to the right.

50–70% of the sediments in other offshore sites are derived from the Indian peninsula and that the rest of the sediments are derived from the Ganges-Brahmaputra River watershed (Kessarkar et al., 2005; Li, Liu, Feng, et al., 2017; Li, Liu, Shi, et al., 2017; Tripathy et al., 2011). During MIS 2 and 4, however, these trace element ratios tend toward more mafic values, suggesting an increased contribution from mafic source rocks.

10.1029/2018GC007772

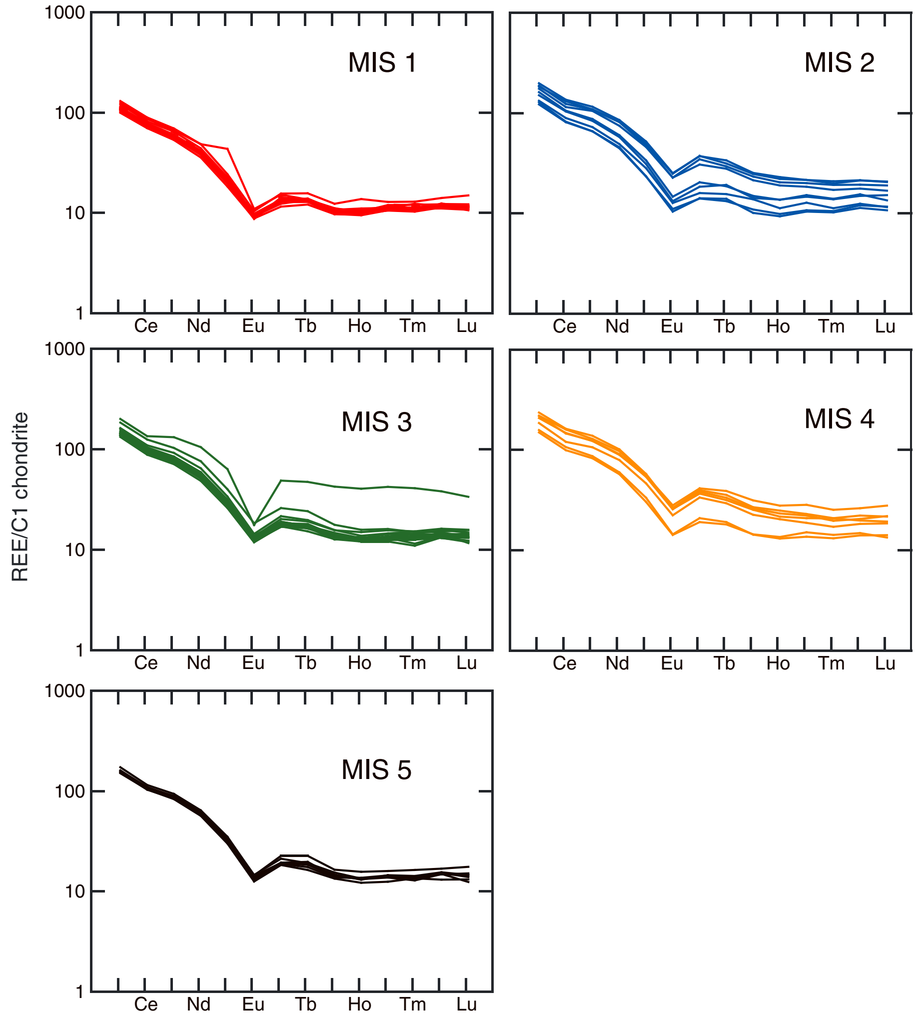

Figure 6. Chondrite-normalized rare earth element (REE) patterns of Hole 19B sediments, grouped by Marine Isotope Stage (MIS).

The REE patterns of source rocks are preserved in clastic sediments (Taylor & McLennan, 1985). Felsic rocks present higher LREE/HREE ratios and negative Eu anomalies, whereas mafic rocks generally present lower LREE/HREE ratios with smaller or absent Eu anomalies (Cullers, 2002; Cullers & Graf, 1983). Hence, REE patterns can help to distinguish between felsic and mafic source rock lithologies of clastic sediments (e.g., Ali et al., 2014; Mazumdar et al., 2015). Chondrite-normalized REE patterns show that the studied sediments are enriched in LREEs, with almost flat HREE profiles and negative Eu anomalies (Figure 6). This result supports the inferred generally felsic source contribution to the sediments at Hole 19B. Eu anomalies are generally considered to derive from the sediment source (McLennan et al., 1993) because of the very low mobility of Eu during weathering and postdepositional diagenesis (Gao & Wedepohl, 1995). Ganges-Brahmaputra sediments have Eu/Eu* values between 0.27 and 0.53 (Singh, 2010), rocks of the PGC show a wide range of Eu/Eu* values between 0.48 and 1.0 (Condie, 1993; Gao & Wedepohl, 1995; Moyen et al., 2003), and Deccan basalts range between 0.83 and 1.07 (Melluso et al., 2004). Hole 19B sediments have Eu anomalies between 0.51 and 0.72 (averaging 0.60, $n = 60$, $\sigma = 0.02$) consistent with a PGC source, which indicates the dominant contribution of felsic source sediment (Figure 5e). The slightly higher Eu anomalies during MIS 2 and 4 suggest an increased contribution from mafic source rocks during glacial periods.

In assessing the cause of increased mafic sediment contributions during MIS 2 and 4, we note that the sediment source area can be influenced by not only the distribution of terrestrial rainfall but also sea surface currents (e.g., Awasthi et al., 2014; Ramaswamy et al., 2004). The weakened summer monsoons during MIS

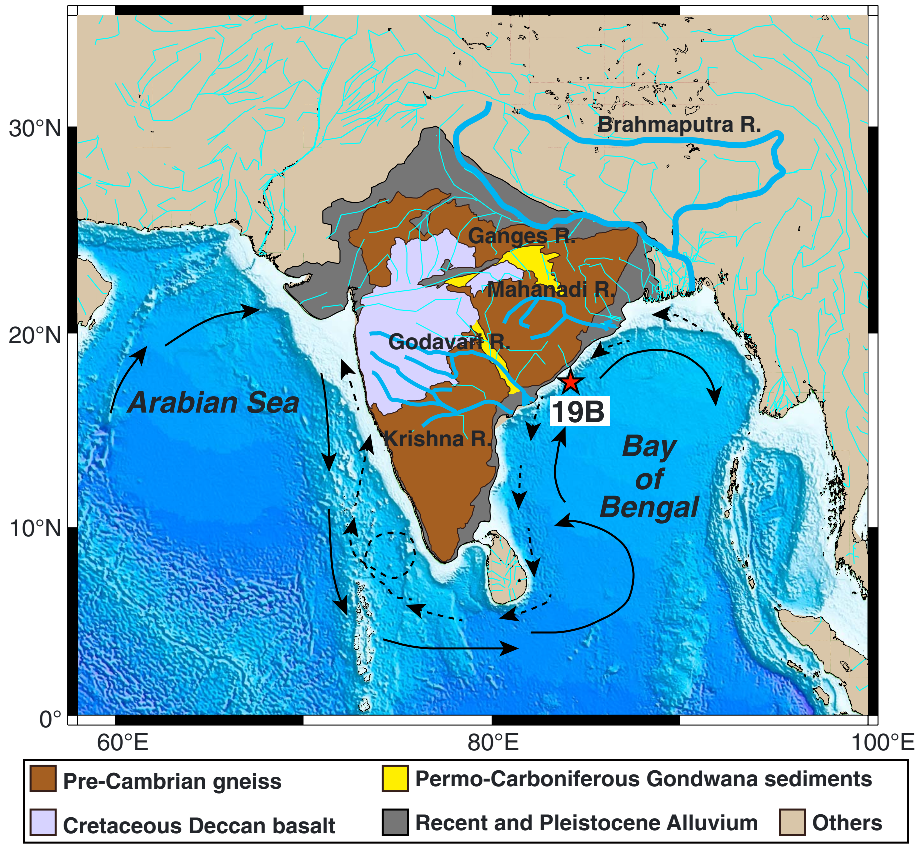

Figure 7. Location map showing Hole 19B in the western Bay of Bengal (red star), the major geologic provinces of the Indian peninsula (simplified from the Geological Survey of India, 2018). Solid and dashed arrows represent the general summer and winter currents, respectively (Schott & McCreary, 2001).

2 and 4 would likely have weakened the clockwise current and enhanced westward sea surface circulations in the Bay of Bengal (e.g., Joussain et al., 2016; Sarkar et al., 1990; Figure 7). If clockwise (eastward) circulations contribute greatly to the transport of sediments from mafic source rocks in the Krishna and Godavari river catchments to our core site, weakened current during MIS 2 and 4 would have reduced that contribution. However, our results show increased mafic contributions during those periods, indicating that changes in oceanic current alone cannot explain the variation of felsic versus mafic sediment contributions at Hole 19B. At present, precipitation is greater in the northeastern and eastern parts of the Indian peninsula than in the western part (Figure 1), and this distribution of rainfall might account for the dominant contribution of felsic sediments to the western Bay of Bengal during MIS 1 shown in this study (Figure 5). Two branches of the summer monsoon deliver moisture to the middle of the Indian peninsula (Gupta et al., 2005): the western branch transports water vapor largely from the Arabian Sea to the western Indian peninsula, and the eastern branch transports water vapor from the Bay of Bengal to the northeastern and eastern parts of the peninsula (Figure 8a). It has been suggested that weaker summer insolation induced a southward displacement of the ITCZ and weaker summer monsoon during MIS 2 and 4 (Clemens & Prell, 2003; Joussain et al., 2016; Kathayat et al., 2016; Stoll et al., 2007) and that the displaced ITCZ shifted the relative influences of the two monsoon branches (e.g., Sarkar et al., 2015). Therefore, the modeling results of Broccoli et al. (2006) indicated that this displaced ITCZ resulted lower precipitation in northeastern and eastern parts of the peninsula and slightly higher precipitation in western parts in MIS 2 in comparison with the present. If the rainfall gradient across the Indian peninsula has been constant during the past 80 kyr, it is expected that the relative contribution of sediments from mafic rocks to our core site should also be constant. On the other hand, if monsoonal precipitation decreased more in the eastern and northeastern Indian peninsula than in the western part, an increased contribution of sediments from mafic source rocks to our core site can be expected via the Krishna-Godavari river system and oceanic currents.

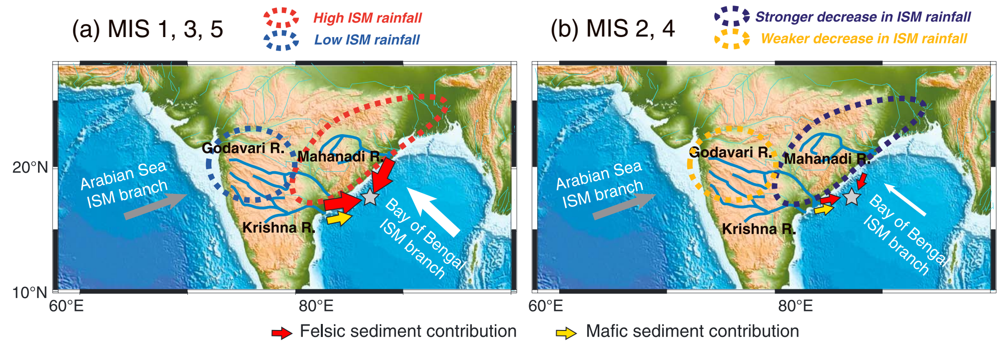

Figure 8. Maps of the Indian peninsula showing areas of sediment provenance, chemical weathering, and Indian summer monsoon (ISM) rainfall (colored dashed lines) inferred for (a) MIS 1, 3, and 5, and (b) MIS 2 and 4. In (b), ISM rainfall is depicted relative to the interglacial rainfall trends in (a). The gray and white arrows represent the Arabian Sea and Bay of Bengal branches of the modern summer monsoon, respectively, and the sizes of the arrows represent the relative influences of the two branches. The size of the colored arrows shows the relative contributions of felsic (red) and mafic (yellow) sediments transported to the site of Hole 19B (gray star).

The increased relative contribution of sediments from western mafic source rocks during MIS 2 and 4 shown in this study may have resulted from a greater decrease in monsoonal precipitation in the eastern and northeastern than the western part of the Indian peninsula during these periods due to the migrated ITCZ (Figure 8b).

The relatively high illite content of Hole 19B sediments indicates the dominantly felsic PGC source of the sediments (Figure 9a). Clay mineral components of the samples plot in the field of Indian PGC source sediments and near that of Ganges-Brahmaputra delta sediments (Figure 9b). Major element ternary A-CN-K and A-CNK-FM diagrams (where A = Al_2O_3, C = CaO, N = Na_2O, K = K_2O, F = Fe_2O_3, and M = MgO; Nesbitt et al., 1996) have been used to identify the effects of weathering and transport processes and sedimentary origins (e.g., Babechuk et al., 2014; Sharma et al., 2013). On both diagrams, our samples plot near the fields of the Indian PGC source sediment in the western Bay of Bengal and weathered gneissic complex sediments in the eastern Indian peninsula (Figured 10a and 10b). This result supports a greater influence of PGC than

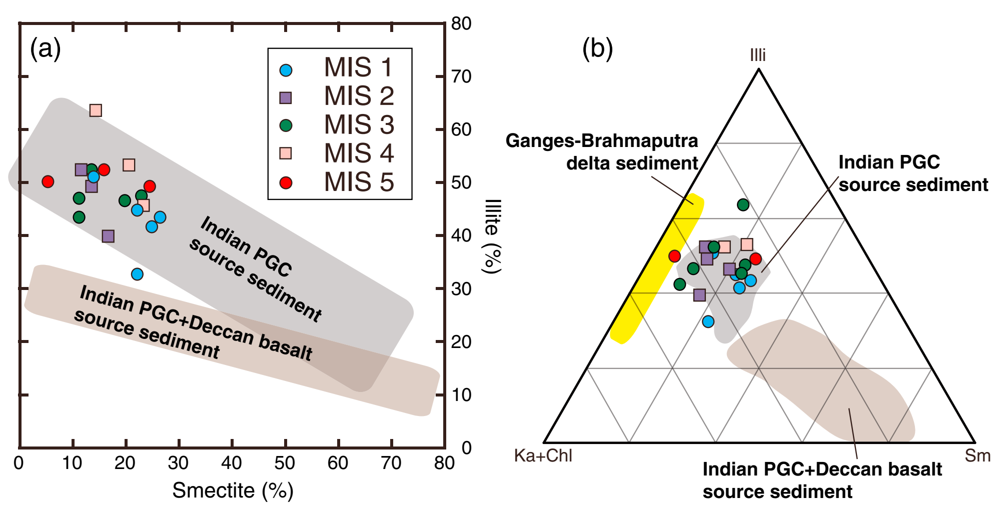

Figure 9. Relative abundances of (a) illite and smectite and (b) illite (Illi), kaolinite plus chlorite (Ka + Chl), and smectite (Sm) in Hole 19B sediments. Sample data are symbolized according to marine isotope stage (MIS), with circles representing interglacial periods (MIS 1, 3, and 5), and squares representing glacial periods (MIS 2 and 4). Reference values of sediments from the Mahanadi (Phillips, Johnson, Underwood, et al., 2014) and Krishna-Godavari basins (Mazumdar et al., 2015) were used to represent the Indian Precambrian Gneiss Complex (PGC) source sediment and combined Indian PGC and Deccan basalt source sediments, respectively. Reference data for Ganges-Brahmaputra delta sediment are from Datta and Subramanian (1997).

10.1029/2018GC007772

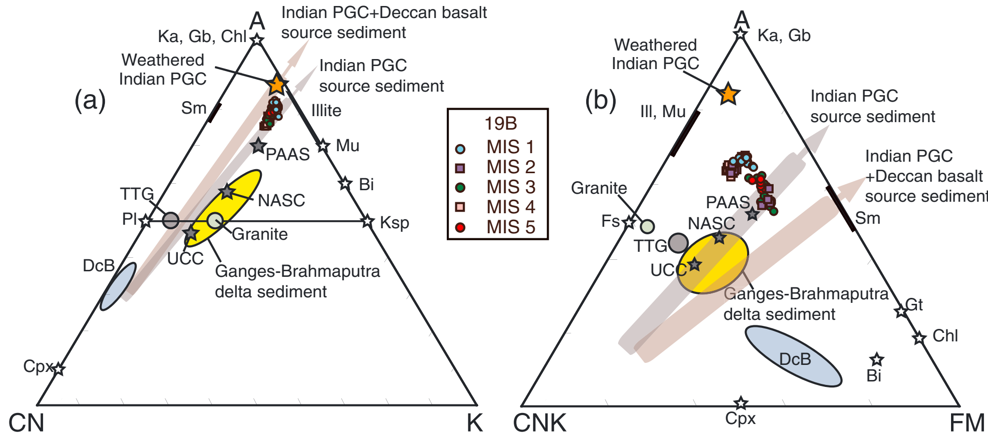

Figure 10. Ternary diagrams showing molar proportions of (a) Al2O3 (A), CaO + Na2O (CN), and K2O (K), and (b) Al2O3 (A), CaO + Na2O + K2O (CNK), and Fe2O3 + MgO (FM) in sediment samples from Hole 19B. Average compositions are plotted for relevant rock-forming minerals, clay minerals, bedrock provinces, and sediment compositions. Abbreviations are as follows: Bi, biotite; Chl, chlorite; Cpx, clinopyroxene; Fs, feldspar; Gb, gibbsite; Gt, garnet; Ka, kaolinite; Ksp, K-feldspar; Mu, muscovite; Pl, plagioclase; Sm, smectite; PGC, Precambrian gneissic complex; DcB, Deccan basalt (Krishnamurthy et al., 2014); NASC, North American shale composition; PAAS, post-Archean average shale; TTG, tonalitic-trondhjemitic-granodioritic compositions of the Indian peninsula (Moyen et al., 2003); and UCC, upper continental crust composition (Taylor & McLennan, 1985). Indian peninsula granite compositions are from Moyen et al. (2003). The weathered PGC sediment composition is taken as A1 of Tripathi and Rajamani (2007). Reference values of sediments from the Mahanadi (Phillips, Johnson, Underwood, et al., 2014) and Krishna-Godavari basins (Mazumdar et al., 2015) were used to represent Indian PGC source sediments (gray shaded arrows) and combined Indian PGC and Deccan basalt source sediments (tan shaded arrows), respectively. Reference data for Ganges-Brahmaputra delta sediments are from Stummeyer et al. (2002).

Himalayan rocks in the provenance of Hole 19B sediments. Clay mineral and major element components do not show the increased contribution from mafic source sediments during MIS 2 and 4. However, because those components, unlike immobile trace elements, are influenced by several factors including weathering and sorting (Armstrong-Altrin et al., 2015), it is likely that the slightly increased contributions of mafic source sediments are not reflected in the clay mineral and major element components.

6. Conclusions

We estimated the sedimentation rate for a sediment core from Hole 19B in the western Bay of Bengal, extending to approximately 80 kyr BP, on the basis of radiocarbon dates and the $\delta^{18}O$ stack record. Considering major and trace element compositions and clay mineral components of the sediments, we arrived at the following conclusions.

1. Low $\delta^{18}O$ values of *G. ruber* s.s., high sedimentation rates, and increased TiO_2 contents during MIS 1, 3, and 5 indicate increased summer monsoonal rainfall in the areas surrounding the western Bay of Bengal. Among these interglacial periods, our results indicate that precipitation was highest during MIS 1.
2. Chemical weathering in the sediment source area, as indicated by the CIA, CIW, and PIA indices, was more intense during MIS 1, 3, and 5 than during MIS 2 and 4. This finding indicates wetter conditions in the sediment source areas during interglacial periods.
3. Trace element ratios (Th/Co, Th/Sc, La/Cr, and Cr/Th) and Eu/Eu* suggest that the Ganges-Brahmaputra watershed and Precambrian gneissic complex in the eastern Indian peninsula have been the dominant source of sediments entering the western Bay of Bengal during the last 80 kyr. Sediment contributions from mafic source rocks slightly increased during MIS 2 and 4.
4. The relatively increased sediment contribution from mafic source rocks during MIS 2 and 4 can be explained by a greater decrease in precipitation in the eastern than in the western Indian peninsula, which may have resulted from shifting influences between the western and eastern branches of the summer monsoon.
5. Clay mineral and chemical compositions suggest that the sediments were sourced more from felsic igneous rocks of the eastern Indian peninsula than from Himalayan rocks.

Acknowledgments

The authors are thankful to the Ministry of Petroleum and Natural Gas within the Government of India, Oil and Natural Gas Corporation Limited (ONGC), Directorate General of Hydrocarbons (DGH), Oil India Ltd, GAIL (India) Ltd, Indian Oil Corporation Ltd, and all other NGHP partner organizations for providing us the opportunity to contribute to the NGHP-02 Expedition. The authors thank the crew of D/V *Chikyu*, drillers, Japanese Drilling Corporation, and JAMSTEC Science Team who contributed to the overall success of NGHP-02 Expedition. Shipboard sampling was done by onboard scientists (including Y. Yamamoto), and onboard technical staff of Marine Work Japan Co. Ltd. (including S. Nigi, T. Yabuki). Part of this work was funded by the Sasakawa Scientific Research Grant from the Japan Science Society. We thank K. Morimoto of AIST for his help with the XRD measurements, N. Ogawa for XRF analyses, T. Ishimura of National Institute of Technology, Ibaraki College, and Y. Yoshinaga of AIST for $\delta^{18}O$ analyses. The data used are listed in the tables, references, and supporting information.

References

Ahmad, S. M., Padmakumari, V. M., & Babu, G. A. (2009). Strontium and neodymium isotopic compositions in sediments from Godavari, Krishna, and Pennar rivers. *Current Science*, *97*(12), 1766–1769.

Alagarsamy, R. (2009). Environmental magnetism and application in the continental shelf sediments of India. *Marine Environmental Research*, *68*, 49–58. https://doi.org/10.1016/j.marenvres.2009.04.003

Ali, S., Stattegger, K., Garbe-Schönberg, D., Frank, M., Kraft, S., & Kuhnt, W. (2014). The provenance of Cretaceous to Quaternary sediments in the Tarfaya basin, SW Morocco: Evidence from trace element geochemistry and radiogenic Nd-Sr isotopes. *Journal of African Earth Sciences*, *90*, 64–76. https://doi.org/10.1016/j.jafrearsci.2013.11.010

Armstrong-Altrin, J. S., & Machain-Castillo, M. L. (2016). Mineralogy, geochemistry, and radiocarbon ages of deep sea sediments from the Gulf of Mexico, Mexico. *Journal of South American Earth Sciences*, *71*, 182–200. https://doi.org/10.1016/j.jsames.2016.07.010

Armstrong-Altrin, J. S., Machain-Castillo, M. L., Rosales-Hoz, L., Carranza-Edwards, A., Sanchez-Cabeza, J. A., & Ruíz-Fernández, A. C. (2015). Provenance and depositional history of continental slope sediments in the southwestern Gulf of Mexico unraveled by geochemical analysis. *Continental Shelf Research*, *95*, 15–26. https://doi.org/10.1016/j.csr.2015.01.003

Awasthi, N., Ray, J. S., Singh, A. K., Band, S. T., & Rai, V. K. (2014). Provenance of the Late Quaternary sediments in the Andaman Sea: Implications for monsoon variability and ocean circulation. *Geochemistry, Geophysics, Geosystems*, *15*, 3890–3906. https://doi.org/10.1002/2014GC005462

Babechuk, M. G., Widdowson, M., & Kamber, B. S. (2014). Quantifying chemical weathering intensity and trace element release from two contrasting basalt profiles, Deccan Traps, India. *Chemical Geology*, *363*, 56–75. https://doi.org/10.1016/j.chemgeo.2013.10.027

Bastia, R. (2007). *Geologic settings and petroleum systems of India's east coast offshore basins: Concepts and applications*. Dehradun, India: Technology Publications.

Bejugam, P., & Nayak, G. N. (2016). Source and depositional processes of the surface sediments and their implications on productivity in recent past off Mahanadi to Pennar River mouths, western Bay of Bengal. *Palaeogeography, Palaeoclimatology, Palaeoecology*, *483*, 58–69. https://doi.org/10.1016/j.palaeo.2016.12.006

Berger, A. L. (1978). Long-term variations of caloric insolation from the Earth's orbital elements. *Quaternary Research*, *9*, 139–167.

Biksham, G., & Subramanian, V. (1988). Sediment transport of the Godavari River basin and its controlling factors. *Journal of Hydrology*, *101*, 275–290. https://doi.org/10.1016/0022-1694(88)90040-6

Biscaye, P. E. (1965). Mineralogy and sedimentation of recent deep-sea clay in the Atlantic Ocean and adjacent seas and oceans. *Geological Society of America Bulletin*, *76*, 803–832.

Blöthe, J. H., & Korup, O. (2013). Millennial lag times in the Himalayan sediment routing system. *Earth and Planetary Science Letters*, *382*, 38–46 . https://doi.org/10.1016/j.epsl.2013.08.044

Broccoli, A. J., Dahl, K. A., & Stouffer, R. J. (2006). Response of the ITCZ to Northern Hemisphere cooling. *Geophysical Research Letters*, *33*, L01702. https://doi.org/10.1029/2005GL024546

Central Water Commission (CWC), & National Remote Sensing Centre (NRSC). (2014a). Krishna basin. Retrieved from http://india-wris.nrsc.gov.in/Publications/BasinReports/Krishna%20Basin.pdf

Central Water Commission (CWC), & National Remote Sensing Centre (NRSC). (2014b). Godavari basin. Retrieved from http://india-wris.nrsc.gov.in/Publications/BasinReports/Godavari%20Basin.pdf

Central Water Commission (CWC), & National Remote Sensing Centre (NRSC). (2014c). Mahanadi basin. Retrieved from http://india-wris.nrsc.gov.in/Publications/BasinReports/Mahanadi%20Basin.pdf

Chakrapani, G. J., & Subramanian, V. (1990a). Preliminary studies on the geochemistry of the Mahanadi River basin, India. *Chemical Geology*, *81*, 241–253. https://doi.org/10.1016/0009-2541(90)90118-Q

Chakrapani, G. J., & Subramanian, V. (1990b). Factors controlling sediment discharge in the Mahanadi basin, India. *Journal of Hydrology*, *117*, 169–185.

Chauhan, O. S., & Vogelsang, E. (2006). Climate induced changes in the circulation and dispersal patterns of the fluvial sources during Late Quaternary in the middle Bengal Fan. *Journal of Earth System Science*, *115*, 379–386. https://doi.org/10.1007/BF02702050

Clemens, S. C., & Prell, W. L. (2003). A 350,000 year summer-monsoon multi-proxy stack from the Owen Ridge, northern Arabian Sea. *Marine Geology*, *201*, 35–51. https://doi.org/10.1016/S0025-3227(03)00207-X

Clift, P. D. (2017). Cenozoic sedimentary records of climate-tectonic coupling in the Western Himalaya. *Progress in Earth and Planetary Science*, *4*, 39. https://doi.org/10.1186/s40645-017-0151-8

Colin, C., Turpin, L., Bertaux, J., Desprairies, A., & Kissel, C. (1999). Erosional history of the Himalayan and Burman ranges during the last two glacial–interglacial cycles. *Earth and Planetary Science Letters*, *171*, 647–660.

Colin, C., Turpin, L., Blamart, D., Frank, N., Kissel, C., & Duchamp, S. (2006). Evolution of weathering patterns in the Indo-Burman Ranges over the last 280 kyr: Effects of sediment provenance on 87 Sr/86 Sr ratios tracer. *Geochemistry, Geophysics, Geosystems*, *7*, Q03007. https://doi.org/10.1029/2005GC000962

Condie, K. C. (1993). Chemical composition and evolution of the upper continental crust: Contrasting results from surface samples and shales. *Chemical Geology*, *104*, 1–37.

Cullers, R. L. (2002). Implications of elemental concentrations for provenance, redox conditions, and metamorphic studies of shales and limestones near Pueblo, CO, USA. *Chemical Geology*, *191*, 305–327. https://doi.org/10.1016/S0009-2541(02)00133-X

Cullers, R. L., Chaudhuri, S., Kilbane, N., & Koch, R. (1979). Rare earths in size fractions and sedimentary rocks of Pennsylvanian-Permian age from the mid-continent of the USA. *Geochimica et Cosmochimica Acta*, *43*, 1285–1302.

Cullers, R. L., & Graf, J. (1983). Rare earth elements in igneous rocks of the continental crust: Intermediate and silicic rocks, ore petrogenesis. In P. Henderson (Ed.), *Rare-Earth Geochemistry*, (pp. 275–312). Amsterdam: Elsevier.

Curray, J. R., Emmel, F. J., & Moore, D. G. (2003). The Bengal Fan: Morphology, geometry, stratigraphy, history and processes. *Marine and Petroleum Geology*, *19*, 1191–1223. https://doi.org/10.1016/S0264-8172(03)00035-7

Datta, D. K., & Subramanian, V. (1997). Texture and mineralogy of sediments from the Ganges-Brahmaputra-Meghna River system in the Bengal Basin, Bangladesh and their environmental implications. *Environmental Geology*, *30*, 181–188.

Dutta, K., Bhushan, R., & Somayajulu, B. L. K. (2001). ΔR correction values for the northern Indian Ocean. *Radiocarbon*, *43*, 483–488.

Einsele, G. (2000). *Sedimentary basin. evolution, facies, and sediment budget* (2nd ed.). Berlin: Springer-Verlag.

Evans, D., Bhatia, R., Stoll, H., & Müller, W. (2015). LA-ICPMS Ba/Ca analyses of planktic foraminifera from the Bay of Bengal: Implications for late Pleistocene orbital control on monsoon freshwater flux. *Geochemistry, Geophysics, Geosystems*, *16*, 2598–2618. https://doi.org/10.1002/2015GC005822

Fedo, C. M., Nesbitt, H. W., & Young, G. M. (1995). Unraveling the effects of potassium metasomatism in sedimentary rocks and paleosols, with implications for paleoweathering conditions and provenance. *Geology*, *23*, 921–924. https://doi.org/10.1130/0091-7613(1995)023<0921:UTEOPM>2.3.CO;2

Feng, R., & Kerrich, R. (1990). Geochemistry of fine-grained clastic sediments in the Archean Abitibi greenstone belt, Canada: Implications for provenance and tectonic setting. *Geochimica et Cosmochimica Acta*, *54*, 1061–1081. https://doi.org/10.1016/0016-7037(90)90439-R

Gadgil, S., Rajeevan, M., & Nanjundiah, R. (2005). Monsoon prediction—Why yet another failure? *Current Science*, *88*, 1389–1400.

Gao, S., & Wedepohl, K. H. (1995). The negative Eu anomaly in Archean sedimentary rocks: Implications for decomposition, age and importance of their granitic sources. *Earth and Planetary Science Letters*, *133*, 81–94.

Garzanti, E., Andò, S., France-Lanord, C., Vezzoli, G., Censi, P., Galy, V., & Najman, Y. (2010). Mineralogical and chemical variability of fluvial sediments. 1. Bedload sand (Ganga-Brahmaputra, Bangladesh). *Earth and Planetary Science Letters*, *299*, 368–381. https://doi.org/10.1016/j.epsl.2010.09.017

Geological Survey of India. (2018). Retrieved from https://www.gsi.gov.in/webcenter/portal/OCBIS?_afrLoop=933622406807556&_adf.ctrl-state=jmriu0vxl_30#!%40%40%3F_afrLoop%3D933622406807556%26_adf.ctrl-state%3Djmriu0vxl_34

Goswami, B. N., Madhusoodanan, M. S., Neema, C. P., & Sengupta, D. (2006). A physical mechanism for the North Atlantic SST influence on the Indian summer monsoon. *Geophysical Research Letters*, *33*, L02706. https://doi.org/10.1029/2005GL024803

Govil, P., & Naidu, P. D. (2011). Variations of Indian monsoon precipitation during the last 32 kyr reflected in the surface hydrography of the Western Bay of Bengal. *Quaternary Science Reviews*, *30*, 3871–3879. https://doi.org/10.1016/j.quascirev.2011.10.004

Guhathakurta, P., & Rajeevan, M. (2008). Trends in the rainfall pattern over India. *International Journal of Climatology*, *28*, 1453–1469.

Gupta, S. K., Deshpande, R. D., Bhattacharya, S. K., & Jani, R. A. (2005). Groundwater δ^{18}O and δD from central Indian Peninsula: Influence of the Arabian Sea and the Bay of Bengal branches of the summer monsoon. *Journal of Hydrology*, *303*, 38–55. https://doi.org/10.1016/j.jhydrol.2004.08.016

Harnois, L. (1988). The CIW index: A new chemical index of weathering. *Sedimentary Geology*, *55*, 319–322. https://doi.org/10.1016/0037-0738(88)90137-6

Hart, G. F. (1999). The deltas of Peninsular India. Retrieved from http://www.geol.lsu.edu/WDD/PUBLICATIONS/HartIndrpt00/india.htm

He, M., Zheng, H., Clift, P. D., Tada, R., Wu, W., & Luo, C. (2015). Geochemistry of fine-grained sediments in the Yangtze River and the implications for provenance and chemical weathering in East Asia. *Progress in Earth and Planetary Science*, *2*(32). https://doi.org/10.1186/s40645-015-0061-6

Hecht, H., & Oguchi, T. (2017). Global evaluation of erosion rates in relation to tectonics. *Progress in Earth and Planetary Science*, *4*, 40. https://doi.org/10.1186/s40645-017-0156-3

Ishimura, T., Tsunogai, U., & Gamo, T. (2004). Stable carbon and oxygen isotopic determination of sub-microgram quantities of $CaCO_3$ to analyze individual foraminiferal shells. *Rapid Communications in Mass Spectrometry*, *18*, 2883–2888.

Jain, S. K., Agarwal, P. K., & Singh, V. P. (2007). *Hydrology and water resources of India*. Netherlands: Springer.

Joussain, R., Colin, C., Liu, Z., Meynadier, L., Fournier, L., Fauquembergue, K., et al. (2016). Climatic control of sediment transport from the Himalayas to the proximal NE Bengal Fan during the last glacial-interglacial cycle. *Quatanary Science Reviews*, *148*, 1–16.

Kathayat, G., Cheng, H., Sinha, A., Spötl, C., Edwards, R. L., Zhang, H., et al. (2016). Indian monsoon variability on millennial-orbital timescales. *Scientific Reports*, *6*(24374). https://doi.org/10.1038/srep24374

Kessarkar, P., Rao, V. P., Ahmad, S. M., Patil, S. K., Kumar, A. A., Babu, G. A., et al. (2005). Changing sedimentary environment during the Late Quaternary: Sedimentological and isotopic evidence from the distal Bengal Fan. *Deep Sea Research Part I: Oceanographic Research Papers*, *52*, 1591–1615.

Kolla, V., & Biscaye, P. (1973). Clay mineralogy and sedimentation in the eastern Indian Ocean. *Deep Sea Research*, *20*, 727–738.

Krishnamurthy, P., Mahoney, J. J., Gopalan, K., & MacDougall, J. D. (2014). Clinopyroxene compositions in the Deccan and Rajmahal Traps and their bearing on magma types and evolution. *Journal of Asian Earth Science*, *84*, 102–117. https://doi.org/10.1016/j.jseaes.2013.09.023

Krishnaswami, S., & Tripathy, G. R. (2012). Chemical and physical erosion of river basins of India: Links to climate and tectonics. *Proceedings of the Indian National Science Academy*, *78*, 299–311.

Kudrass, H. R., Holfmann, A., Doose, H., Emis, K., & Erlenkuser, H. (2001). Modulation and amplification of climatic changes in the northern hemisphere by the Indian summer monsoon during the past 80 k.y. *Geology*, *29*, 63–66.

Lamb, A. L., Wilson, G. P., & Leng, M. J. (2006). A review of coastal palaeoclimate and relative sea-level reconstructions using δ^{13}C and C/N ratios in organic material. *Earth-Science Reviews*, *75*, 29–57.

Lea, D. W., Pak, D. K., & Spero, H. J. (2000). Climate impact of Late Quaternary equatorial Pacific sea surface temperature variations. *Science*, *289*, 1719–1724. https://doi.org/10.1126/science.289.5485.1719

Li, J., Liu, S., Feng, X., Sun, X., & Shi, X. (2017). Major and trace element geochemistry of the mid-Bay of Bengal surface sediments: Implications for provenance. *Acta Oceanologica Sinica*, *36*, 82–90. https://doi.org/10.1007/s13131-017-1041-z

Li, J., Liu, S., Shi, X., Feng, X., Fang, X., Cao, P., et al. (2017). Distributions of clay minerals in surface sediments of the middle Bay of Bengal: Source and transport pattern. *Continental Shelf Research*, *145*, 59–67. https://doi.org/10.1016/j.csr.2017.06.017

Limmer, D. R., Böning, P., Giosan, L., Ponton, C., Köhler, C. M., Cooper, M. J., et al. (2012). Geochemical record of Holocene to recent sedimentation on the Western Indus continental shelf, Arabian Sea. *Geochemistry, Geophysics, Geosystems*, *13*, Q01008. https://doi.org/10.1029/2011GC003845

Lisiecki, L. E., & Lisiecki, P. A. (2002). Application of dynamic programming to the correlation of paleoclimate records. *Paleoceanography*, *17*(4), 1049. https://doi.org/10.1029/2001PA000733

Lisiecki, L. E., & Raymo, M. E. (2005). A Pliocene-Pleistocene stack of 57 globally distributed benthic δ^{18}O records. *Paleoceanography*, *20*, PA1003. https://doi.org/10.1029/2004PA001071

Malik, N., Bookhagen, B., Marwan, N., & Kurths, J. (2012). Analysis of spatial and temporal extreme monsoonal rainfall over South Asia using complex networks. *Climate Dynamics*, *39*, 971–987.

Mazumdar, A., Peketi, A., Joao, H. M., Dewangan, P., Ramprasad, T., Mahalaxmi, P., et al. (2015). Geochemical characterization of the Krishna-Godavari and Mahanadi offshore basin (Bay of Bengal) sediments: A comparative study of provenance. *Marine and Petroleum Geology*, *60*, 18–33. https://doi.org/10.1016/j.marpetgeo.2014.09.005

McLennan, S. M., Hemming, S., McDaniel, D. K., & Hanson, G. N. (1993). Geochemical approaches to sedimentation, provenance, and tectonics. *Special Papers – Geological Society of America*, *284*, 21–40. https://doi.org/10.1130/SPE284-p21

Meert, J. G., Pandit, M. K., Pradhan, V. R., Banks, J., Sirianni, R., Stroud, M., et al. (2010). Precambrian crustal evolution of Peninsular India: A 3.0 billion year odyssey. *Journal of Asian Earth Sciences*, *39*, 483–515. https://doi.org/10.1016/j.jseaes.2010.04.026

Melluso, L., Barbieri, M., & Beccaluva, L. (2004). Chemical evolution, petrogenesis, and regional chemical correlations of the flood basalt sequence in the central Deccan Traps, India. *Journal of Earth System Science*, *113*, 587–603.

10.1029/2018GC007772

Milliman, J. D. (2001). River inputs. In J. H. Steele, S. A. Thorpe, & K. K. Turekian (Eds.), *Encyclopedia of Ocean Sciences* (pp. 754–761). San Diego, CA: Academic Press.

Milliman, J. D., & Syvitski, J. P. M. (1992). Geomorphic/tectonic control of sediment discharge to the ocean: The importance of small mountainous rivers. *The Journal of Geology*, *100*, 525–544.

Miriyala, P., Sukumaran, N. P., Nath, B. N., Ramamurty, P. B., Sijinkumar, A. V., Vijayagopal, B., et al. (2017). Increased chemical weathering during the deglacial to mid-Holocene summer monsoon intensification. *Scientific Reports*, *7*, 44,310. https://doi.org/10.1038/srep44310

Moyen, J.-F., Martin, H., Jayananda, M., & Auvray, B. (2003). Late Archaean granites: A typology based on the Dharwar Craton (India). *Precambrian Research*, *127*, 103–123. https://doi.org/10.1016/S0301-9268(03)00183-9

Nesbitt, H. W., & Young, G. M. (1982). Early Proterozoic climates and plate motions inferred from major element chemistry of lutites. *Nature*, *299*, 715–717.

Nesbitt, H. W., & Young, G. M. (1984). Prediction of some weathering trends of plutonic and volcanic rocks based on thermodynamic and kinetic considerations. *Geochimica et Cosmochimica Acta*, *48*, 1523–1534. https://doi.org/10.1016/0016-7037(84)90408-3

Nesbitt, H. W., Young, G. M., McLennan, S. M., & Keays, R. R. (1996). Effects of chemical weathering and sorting on the petrogenesis of siliciclastic sediments, with implications for provenance studies. *Journal of Geology*, *104*, 525–542. https://doi.org/10.1086/629850

Ota, Y., Kawahata, H., Murayama, M., Inoue, M., Yokoyama, Y., Miyairi, Y., et al. (2017). Effects of intensification of the Indian summer monsoon on northern Andaman Sea sediments during the past 700 years. *Journal of Quatanary Science*, *32*, 528–539. https://doi.org/10.1002/jqs.2947

Phillips, S. C., Johnson, J. E., Giosan, L., & Rose, K. (2014). Monsoon-influenced variation in productivity and lithogenic sediment flux since 110 ka in the offshore Mahanadi Basin, northern Bay of Bengal. *Marine and Petroleum Geology*, *58*, 502–525. https://doi.org/10.1016/j.marpetgeo.2014.05.007

Phillips, S. C., Johnson, J. E., Underwood, M. B., Guo, J., Giosan, L., & Rose, K. (2014). Long-timescale variation in bulk and clay mineral composition of Indian continental margin sediments in the Bay of Bengal, Arabian Sea, and Andaman Sea. *Marine and Petroleum Geology*, *58*, 117–138. https://doi.org/10.1016/j.marpetgeo.2014.06.018

Ponton, C., Giosan, L., Eglinton, T. I., Fuller, D. Q., Johnson, J. E., Kumar, P., & Collett, T. S. (2012). Holocene aridification of India. *Geophysical Research Letters*, *39*, L03704. https://doi.org/10.1029/2011GL050722

Prasanna Kumar, S., Nuncio, M., Ramaiah, N., Sardesai, S., Narvekar, J., Fernandes, V., & Paul, J. T. (2007). Eddy-mediated biological productivity in the Bay of Bengal during fall and spring intermonsoons. *Deep Sea Research, Part I*, *54*, 1619–1640. https://doi.org/10.1016/j.dsr.2007.06.002

Rahaman, M. M., & Varis, O. (2009). Integrated water management of the Brahmaputra basin: Perspectives and hope for regional development. *Natural Resources Forum*, *33*(1), 60–75. https://doi.org/10.1111/j.1477-8947.2009.01209.x

Rahman, M. J. J., & Suzuki, S. (2007). Geochemistry of sandstones from the Miocene Surma group, Bengal Basin, Bangladesh: Implications for provenance, tectonic setting and weathering. *Geochemical Journal*, *41*, 415–428.

Ramaswamy, V., Rao, P. S., Rao, K. H., Thwin, S., Rao, N. S., & Raiker, V. (2004). Tidal influence on suspended sediment distribution and dispersal in the northern Andaman Sea and Gulf of Martaban. *Marine Geology*, *208*, 33–42. https://doi.org/10.1016/j.margeo.2004.04.019

Ramesh, R., Subramanian, V., Van Grieken, R., & Van't Dack, L. (1989). The elemental chemistry of sediments in the Krishna River basin, India. *Chemical Geology*, *74*, 331–341. https://doi.org/10.1016/0009-2541(89)90042-9

Rao, G. N. (2001). Sedimentation, stratigraphy, and petroleum potential of Krishna-Godavari basin, east coast of India. *AAPG Bulletin*, *85*, 1623–1643. https://doi.org/10.1306/8626CCDF-173B-11D7-8645000102C1865D

Rao, V. P. (1991). Clay mineral distribution in the continental shelf sediments from Krishna to Ganges River mouth, east coast of India. *Indian Journal of Marine Sciences*, *20*, 7–12.

Rao, V. P., & Nath, B. N. (1988). Nature, distribution and origin of clay minerals in grain size fractions of sediments from manganese nodule field, central Indian Ocean basin. *Indian Journal of Marine Sciences*, *17*, 202–207.

Rashid, H., England, E., Thompson, L., & Polyak, L. (2011). Late Glacial to Holocene Indian summer monsoon variability based upon sediment records taken from the Bay of Bengal. *Terrestrial, Atmospheric and Oceanic Sciences*, *22*, 215–228. https://doi.org/10.3319/TAO.2010.09.17.02(TibXS)

Rashid, H., Flower, B. P., Poore, R. Z., & Quinn, T. M. (2007). A ~25 ka Indian Ocean monsoon variability record from the Andaman Sea. *Quatanary Science Reviews*, *26*, 2586–2597.

Reimer, P. J., Bard, E., Bayliss, A., Beck, J. W., Blackwell, P. G., & Ramsey, C. B. (2013). IntCal13 and Marine13 radiocarbon age calibration curves 0–50,000 years cal BP. *Radiocarbon*, *55*, 1869–1887. https://doi.org/10.2458/azu_js_rc.55.16947

Saito, K., Tada, R., Zheng, H., Irino, T., Luo, C., He, M., et al. (2017). ESR signal intensity of quartz in the fine-silt fraction of riverbed sediments from the Yangtze River: A provenance tracer for suspended particulate matter. *Progress in Earth and Planetary Science*, *4*, 4. https://doi.org/10.1186/s40645-017-0118-9

Sarkar, A., Ramesh, R., Bhattacharya, S. K., & Rajagopalan, G. (1990). Oxygen isotope evidence for a stronger winter monsoon during the last glaciation. *Nature*, *343*, 549–551.

Sarkar, S., Prasad, S., Wilkes, H., Riedel, N., Stebich, M., Basavaiah, N., & Sachse, D. (2015). Monsoon source shifts during the drying mid-Holocene: Biomarker isotope based evidence from the core 'monsoon zone' (CMZ) of India. *Quatanary Science Reviews*, *123*, 144–157.

Schmitz, B. (1987). The TiO_2 Al_2O_3 ratio in the Cenozoic Bengal Abyssal Fan sediments and its use as a paleostream energy indicator. *Marine Geology*, *76*, 195–206. https://doi.org/10.1016/0025-3227(87)90029-6

Schott, F. A., & McCreary, J. P. (2001). The monsoon circulation of the Indian Ocean. *Progress in Oceanography*, *51*, 1–123. https://doi.org/10.1016/S0079-6611(01)00083-0

Scudder, R. P., Murray, R. W., Schindlbeck, J. C., Kutterolf, S., Hauff, F., Underwood, M. B., et al. (2016). Geochemical approaches to the quantification of dispersed volcanic ash in marine sediment. *Progress in Earth and Planetary Science*, *3*, 1. https://doi.org/10.1186/s40645-015-0077-y

Sengupta, S., Parekh, A., Chakraborty, S., Ravi Kumar, K., & Bose, T. (2013). Vertical variation of oxygen isotope in Bay of Bengal and its relationships with water masses. *Journal of Geophysical Research: Oceans*, *118*, 6411–6424. https://doi.org/10.1002/2013JC008973

Seto, M., & Akagi, T. (2008). Chemical condition for the appearance of a negative Ce anomaly in stream waters and groundwaters. *Geochemical Journal*, *42*, 371–380.

Sharma, A., Sensarma, S., Kumar, K., Khanna, P. P., & Saini, N. K. (2013). Mineralogy and geochemistry of the Mahi River sediments in tectonically active western India: Implications for Deccan large igneous province source, weathering and mobility of elements in a semi-arid climate. *Geochimica et Cosmochimica Acta*, *104*, 63–83. https://doi.org/10.1016/j.gca.2012.11.004

Shukla, A. D., Bhandari, N., Kusumgar, S., Shukla, P. N., Ghevariya, Z. G., Gopalan, K., & Balaram, V. (2001). Geochemistry and magnetostratigraphy of Deccan flows at Anjar, Kutch. *Proceedings of the Indian Academy of Sciences, Earth and Planetary Sciences*, *110*, 111–132. https://doi.org/10.1007/BF02702212

Sijinkumar, A. V. (2016). $\delta^{18}O$ and salinity variability from the Last Glacial Maximum to recent in the Bay of Bengal and Andaman Sea. *Quaternary Science Reviews*, *135*, 79–91. https://doi.org/10.1016/j.quascirev.2016.01.022

Singh, M., Singh, I. B., & Müller, G. (2007). Sediment characteristics and transportation dynamics of the Ganga River. *Geomorphology*, *86*, 144–175. https://doi.org/10.1016/j.geomorph.2006.08.011

Singh, P. (2010). Geochemistry and provenance of stream sediments of the Ganga River and its major tributaries in the Himalayan region, India. *Chemical Geology*, *269*, 220–236.

Singh, S. K., Sarin, M. M., & France-Lanord, C. (2005). Chemical erosion in the eastern Himalaya: Major ion composition of the Brahmaputra and $\delta^{13}C$ of the dissolved inorganic carbon. *Geochimica et Cosmochimica Acta*, *69*, 3573–3588.

Sinha, A., Cannariato, K. G., Stott, L. D., Cheng, H., Edwards, R. L., Yadava, M. G., et al. (2007). A 900-year (600 to 1500 A.D.) record of the Indian summer monsoon precipitation from the core monsoon zone of India. *Geophysical Research Letters*, *34*, L16707. https://doi.org/10.1029/2007GL030431

Southon, J., Kashgarian, M., Fontugne, M., Metivier, B., & Yim, W. W.-S. (2002). Marine reservoir corrections for the Indian Ocean and Southeast Asia. *Radiocarbon*, *44*, 167–180.

Spero, H. J., Mielke, K. M., Kalve, E. M., Lea, D. W., & Pak, D. K. (2003). Multispecies approach to reconstructing eastern equatorial Pacific thermocline hydrography during the past 360 kyr. *Paleoceanography*, *18*(1), 1022. https://doi.org/10.1029/2002PA000814

Stoll, H. M., Vance, D., & Arevalos, A. (2007). Records of the Nd isotope composition of seawater from the Bay of Bengal: Implications for the impact of Northern Hemisphere cooling on ITCZ movement. *Earth and Planetary Science Letters*, *255*, 213–228. https://doi.org/10.1016/j.epsl.2006.12.016

Storey, M., Roberts, R. G., & Saidin, M. (2012). Astronomically calibrated $^{40}Ar/^{39}Ar$ age for the Toba supereruption and global synchronization of late Quaternary records. *Proceedings of the National Academy of Sciences*, *109*, 18,684–18,688.

Stuiver, M., Reimer, P. J., & Reimer, R. W. (2017). CALIB 7.1 [WWW program], Retrieved at http://calib.org [2017-12-12].

Stummeyer, J., Marchig, V., & Knabe, W. (2002). The composition of suspended matter from Ganges-Brahmaputra sediment dispersal system during low sediment transport season. *Chemical Geology*, *185*, 125–147. https://doi.org/10.1016/S0009-2541(01)00396-5

Subramanian, V. (1980). Mineralogical input of suspended matter by Indian rivers into the adjacent areas of the Indian Ocean. *Marine Geology*, *36*, 29–34. https://doi.org/10.1016/0025-3227(80)90084-5

Subramanian, V. (1993). Sediment load of Indian rivers. *Current Science*, *64*, 928–930.

Suzuki, Y., Tada, R., Yamada, K., Irino, T., Nagashima, K., Nakagawa, T., & Omori, T. (2016). Mass accumulation rate of detrital materials in Lake Suigetsu as a potential proxy for heavy precipitation: A comparison of the observational precipitation and sedimentary record. *Progress in Earth and Planetary Science*, *3*, 5. https://doi.org/10.1186/s40645-016-0081-x

Tada, R., & Murray, R. W. (2016). Preface for the article collection "Land–ocean linkages under the influence of the Asian monsoon". *Progress in Earth and Planetary Science*, *3*, 24. https://doi.org/10.1186/s40645-016-0100-y

Tada, R., Zheng, H., & Clift, P. D. (2016). Evolution and variability of the Asian monsoon and its potential linkage with uplift of the Himalaya and Tibetan Plateau. *Progress in Earth and Planetary Science*, *3*, 4. https://doi.org/10.1186/s40645-016-0080-y

Takahashi, N., Taniuchi, T., Abe, K., Sato, T., & Sugitani, T. (2008). *Introduction to geography*. Tokyo: Kokon-syoinn.

Taylor, S. R., & McLennan, S. (1985). *The continental crust: Its composition and evolution*. Oxford, UK: Blackwell Scientific Publications.

Tiwari, M., Ramesh, R., Somayajulu, B. L. K., Jull, A. J. T., & Burr, G. S. (2005). Solar control of southwest monsoon on centennial timescales. *Current Science*, *89*, 1583–1589.

Tripathi, J. K., & Rajamani, V. (2007). Geochemistry and origin of ferruginous nodules in weathered granodioritic gneisses, Mysore Plateau, Southern India. *Geochimica et Cosmochimica Acta*, *71*, 1674–1688. https://doi.org/10.1016/j.gca.2007.01.001

Tripathy, G. R., Singh, S. K., Bhushan, R., & Ramaswamy, V. (2011). Sr-Nd isotope composition of the Bay of Bengal sediments: Impact of climate on erosion in the Himalaya. *Geochemical Journal*, *45*, 175–186. https://doi.org/10.2343/geochemj.1.0112

Tripathy, G. R., Singh, S. K., & Ramaswamy, V. (2014). Major and trace element geochemistry of Bay of Bengal sediments: Implications to provenances and their controlling factors. *Palaeogeography, Palaeoclimatology, Palaeoecology*, *397*, 20–30.

Webster, P. J. (1987). The elementary monsoon. In J. S. Fein & P. L. Stephens (Eds.), *Monsoons* (pp. 3–32). New York: John Wiley.

Wei, G., Liu, Y., Li, X., Shao, L., & Liang, X. (2003). Climatic impact on Al, K, Sc and Ti in marine sediments: Evidence from ODP site 1144, South China Sea. *Geochemical Journal*, *37*, 593–602. https://doi.org/10.2343/geochemj.37.593

Yamamoto, Y., Chiyonobu, S., Kanamatsu, T., Ahagon, N., Aoike, K., Kamiya, N., et al., & NGHP-02 Scientists (2018). Repeated large-scale mass-transport deposits and consequent rapid sedimentation in the western part of the Bay of Bengal. *Geological Society, London, Special Publications*, *477*. https://doi.org/10.1144/SP477.12

Yamasaki, T., & Yamashita, K. (2016). Whole rock multiple trace element analyses using fused glass bead by laser ablation-ICP-MS. *Bulletin of the Geological Survey of Japan*, *67*, 27–40.

Yarincik, K. M., Murray, R. W., & Peterson, L. C. (2000). Climatically sensitive eolian and hemipelagic deposition in the Cariaco Basin, Venezuela, over the past 578,000 years: Results from Al/Ti and K/Al. *Paleoceanography*, *15*(2), 210–228. https://doi.org/10.1029/1999PA900048